Stable, High-Order and Conservative Cut-Cell Methods

P. T. Brady* and D. Livescu.†
Los Alamos National Laboratory, Los Alamos, NM, 87544

Cut-cell methods allow for the use of Cartesian meshes to resolve phenomena occurring in complex geometries. The advantage of cut-cell methods over approaches requiring body fitted meshes (either structured or unstructured) is that the former do not require a costly mesh generation step. However, cut-cell methods have been limited to low orders of accuracy. This is driven, largely, by the variety of procedures typically introduced to evaluate derivatives in a stable manner near the highly irregular embedded geometry. In the present work, a completely new approach is taken to solve this problem. The approach is based on two simple and intuitive design principles. These principles allow for the construction of stable 8^{th} order approximations to parabolic and elliptic problems and stable and conservative 5^{th} order approximations to hyperbolic problems. To the best of the authors' knowledge, these schemes are the highest orders achieved for a cut-cell discretization by a significant margin. This is accomplished without any geometric transformations or artificial stabilization procedures.

I. Nomenclature

Ω_s	=	solid domain
Ω_f	=	fluid domain
Γ_f	=	boundary of fluid domain
Γ_s	=	boundary of solid domain
h	=	distance between points on uniform mesh
ψ	=	fractional distance between Γ_s and first point in Ω_f in coordinate direction
$\boldsymbol{A}$	=	bold capital letters represent matrices
F	=	regular capital letters represent column vectors

II. Introduction

The cut-cell method [1] allows for the solution of partial differential equations (PDEs) defined on complicated domains to be computed numerically on simple Cartesian meshes. This method has seen extensive use in the fluids community, so we define the domain of interest, Ω_f, as the fluid domain which is bounded by $\Gamma_f \cup \Gamma_s$, where the Cartesian and solid object boundaries are given by Γ_f and Γ_s, respectively. A schematic of this is shown in Fig. 1. Thus, the non-Cartesian physical boundaries are embedded into the simpler Cartesian mesh leading to computational cells which have been cut by the embedded object. Rather than modifying the physical equations to implicitly account for this object, the cut-cell approach modifies the discrete derivative operators and imposes boundary conditions directly on Γ_s.

The allure of cut-cell type methods has attracted the attention and effort of a number of researchers for many years (see [2] for a review). In theory, cut-cell methods obviate the need for unstructured meshes and allow for the use of robust, accurate and conservative finite difference/volume schemes with only slight modifications near the boundary. However, the current solutions to the severe numerical challenges of cut-cell schemes typically lead to significant modifications of both the discrete algorithms and the physical equations. The discrete algorithms are modified by requiring significant extra procedures to evaluate derivatives near the boundary since a straightforward evaluation leads to instabilities. The physical equations are typically modified by requiring some sort of stabilization procedure which manifests itself as a source term in the governing equations (even if not explicitly written as such).

The numerical difficulties facing cut-cell methods, warranting these kinds of modifications, are three-fold:

1) Evaluation of spatial derivatives on meshes where at least one point on Γ_s is arbitrarily close to a fluid point in Ω_f (termed a "degenerate mesh" herein) without compromising stability.

*Scientist, CCS-2, MS-D413, Member
†Scientist, CCS-2, MS-D413, Associate Fellow

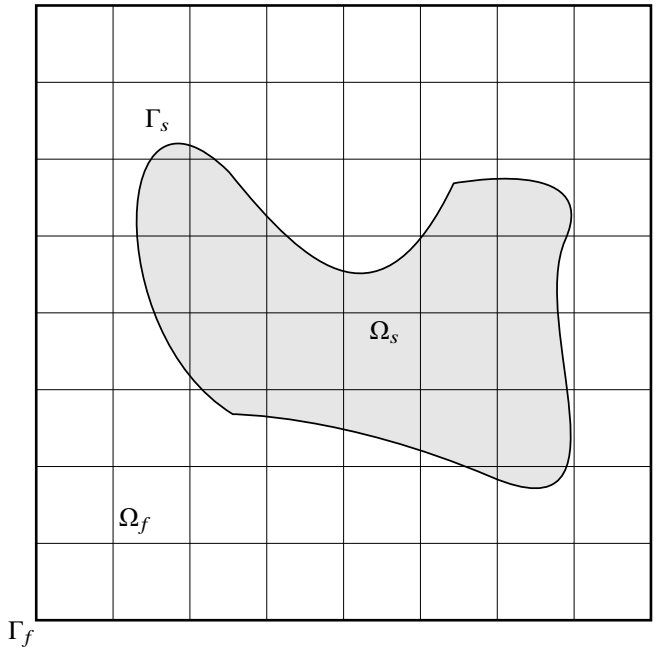

Fig. 1 Schematic of solid object, bounded by Γ_s, embedded in a fluid domain, Ω_f, with Cartesian boundaries Γ_f.

2) Robust and accurate interpolation of field data to evaluate spatial gradients at the boundary.

3) Robust and accurate handling of computational cells whose fluid/solid geometry varies with time.

A solution to item 2 is required for a multi-dimensional Γ_s where the governing equations are to be solved along Γ_s (i.e. problems involving Neumann boundary conditions). A solution to item 3 is required for applying the cut-cell approach to moving objects. In the present work, we focus exclusively on item 1 (known as the "small-cell problem") as this is the foundation on which a complete cut-cell method can successfully address items 2 and 3.

The small-cell problem is illustrated in one dimension in Fig. 2, where an otherwise uniform mesh of constant spacing, h, has an embedded wall on the left side of the domain such that the distance between the wall, Γ_s, and the first fluid point is ψh with $\psi \in [0, 1]$. When $\psi = 1$, the embedded wall coincides with the Cartesian boundary on the left and the mesh spacing becomes uniform. As $\psi \to 0$, the embedded wall approaches the first fluid point in the domain leading to a degenerate mesh and the so called "small-cell problem". To the best of the authors' knowledge, every cut-cell scheme that has been devised for unsteady flows, attempts to alleviate this problem through either geometric manipulations to remove the small cells or some kind of stabilizing dynamic procedure which depends on the value of the solution at any given time [1, 3–31]. That is, it is the conventional wisdom that *something* must be done about small cells. In this work, we pursue a different strategy and devise schemes which are stable over the range $\psi \in [0, 1]$ (with $\psi \to 0$ representing the strongest challenge to stability and accuracy) without any geometric modifications or dynamic procedures or stabilizing source terms. In other words, small cells are not a problem for the cut-cell discretizations presented in this paper.

The order of accuracy of cut-cell schemes for unsteady problems has been largely limited to 2^{nd} order [1, 3–27, 29]. To the best of our knowledge, the scheme of [28] for incompressible flows (which was extended to compressible flows in [30]) is the only one which has demonstrated 3^{rd} order accuracy for unsteady problems. However, Ref. [28] mentions that the dynamic correction procedure yields schemes which are unstable in the inviscid limit. To remedy this, dissipative schemes are used in [30] to extend the method to compressible flow.

In this work a fundamentally different strategy is demonstrated, which allows for constructing stable 8^{th} order schemes.

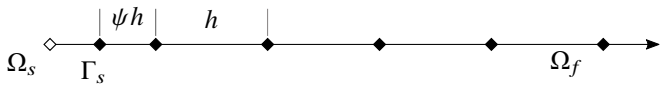

Fig. 2 Solid domain, Ω_s, on the left, with boundary Γ_s. The fluid domain is on the right of Γ_s. The challenge of cut-cell discretizations is to compute stable derivatives near Γ_s over the range $\psi \in [0,1]$. The "small-cell problem" corresponds to small values of ψ.

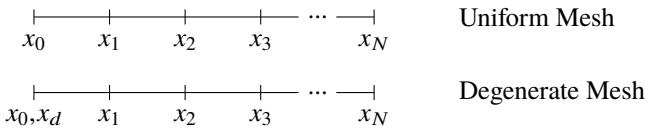

Fig. 3 Uniform mesh with $N+1$ equidistant points and a corresponding degenerate mesh with degenerate point x_d collocated with the left wall at x_0.

III. Construction of Embedded Stencils

While the cut-cell schemes presented in this paper are simple, their construction involves several steps. These steps are described in detail in Ref. [32]. The discussion of the design principles which motivate the novel discretizations are discussed below. The discussion of conservation constraints found in Ref. [32] is not repeated here. The extension of the optimization procedure of Ref. [33] to cut-cell discretizations, which is critical to the design of high-order, non-dissipative schemes for hyperbolic problems, is also not reviewed here. Examples of optimized schemes are given in tables 1-8.

A. Design Principles

The design of our discretization strategy is driven by two simple principles:

1) Given a uniform mesh, the addition of a degenerate point at a wall should not change the truncation error at any point.
2) Do not violate the Taylor series.

The first principle is based on the observation of Schneiders et al. [27], described in the context of moving Γ_s: the solution deteriorates (i.e. oscillations develop) when small changes in Γ_s result in abrupt changes in truncation error which then act as essentially discontinuous forcing terms. The first principle ensures that small changes in Γ_s result in small changes in the truncation error of the scheme.

To focus the discussion of the design principles, consider a domain of length L subject to two different discretizations as shown in Fig. 3. The first discretization uses $N+1$ equidistant points resulting in a uniform mesh of spacing h (labeled "Uniform Mesh" in Fig 3). The second uses the same $N+1$ points as the uniform case but contains an additional degenerate point, x_d, collocated with the left wall at x_0 (labeled "Degenerate Mesh" in Fig 3). Clearly, the addition of the degenerate point only impacts the schemes near the wall. A discrete approximation of order q of the ν^{th} order derivative of some function, f, defined on the grid and evaluated at a point, i, near the boundary is given by:

$$f_i^{(\nu)} = \frac{1}{h^\nu} \sum_{j=0}^{t-1} \alpha_{ij}^u f_j, \tag{1}$$

$$f_i^{(\nu)} = \frac{1}{h^\nu} \left[\alpha_{id}^d f_d + \sum_{j=0}^{t-1} \alpha_{ij}^d f_j \right], \tag{2}$$

where d and u superscripts indicate terms on the degenerate and uniform meshes, respectively. In the interior of the domain, standard central schemes will be used. For these schemes, a stencil of order $2p$ and centered at point i on a grid with constant spacing h, has the form,

$$f_i^{(\nu)} = \frac{1}{h^\nu} \sum_{j=-p}^{j=p} \gamma_j f_{i+j} + O\left(h^{2p}\right), \tag{3}$$

On the uniform mesh, this gives rise to the matrix system:

$$F^{\nu,u} = \frac{1}{h^\nu} \boldsymbol{A}^u F^u, \tag{4}$$

where F^u is the column vector of f_j given by: $F^u = [f_0, f_1, f_2, \ldots, f_N]^T$, and the upper left portion of $\boldsymbol{A}^u$ is:

$$\boldsymbol{A}^u = \begin{bmatrix} \alpha^u_{00} & \alpha^u_{01} & \cdots & \alpha^u_{0,t-1} & & & \\ \vdots & \vdots & \cdots & \vdots & & & \\ \alpha^u_{r-1,0} & \alpha^u_{r-1,1} & \cdots & \alpha^u_{r-1,t-1} & & & \\ & \gamma_{-p} & \gamma_{-(p-1)} & \cdots & \gamma_{p-1} & \gamma_p & \\ & & \ddots & \ddots & \ddots & \ddots & \ddots \end{bmatrix}, \tag{5}$$

The coefficients of $\boldsymbol{A}^u$ are determined, in part, by Taylor series analysis. The width of the boundary stencils can be adjusted to allow for free parameters which can be determined by the optimization process of [32]. On the degenerate mesh, the matrix system is:

$$F^{\nu,d} = \frac{1}{h^\nu} \boldsymbol{A}^d F^d, \tag{6}$$

where F^d is the column vector of f_j given by: $F^d = [f_0, f_d, f_1, f_2, \ldots, f_N]^T$, and the upper left portion of $\boldsymbol{A}^d$ is:

$$\boldsymbol{A}^d = \begin{bmatrix} \alpha^d_{00} & \alpha^d_{01} & \cdots & \alpha^d_{0,t} & & & \\ \vdots & \vdots & \cdots & \vdots & & & \\ \alpha^d_{r,0} & \alpha^d_{r,1} & \cdots & \alpha^d_{r,t} & & & \\ & \gamma_{-p} & \gamma_{-(p-1)} & \cdots & \gamma_{p-1} & \gamma_p & \\ & & \ddots & \ddots & \ddots & \ddots & \ddots \end{bmatrix}, \tag{7}$$

For the truncation errors associated with $F^{\nu,u}$ and $F^{\nu,d}$ to match, as well maintaining the assumptions of continuity inherent in finite differrence approximations, the coefficients of $\boldsymbol{A}^d$ are given in terms of $\boldsymbol{A}^u$ as:

$$\boldsymbol{A}^d = \begin{bmatrix} \alpha^u_{00} & 0 & \alpha^u_{01} & \cdots & \alpha^u_{0,t-1} & & & \\ \alpha^u_{00} & 0 & \alpha^u_{01} & \cdots & \alpha^u_{0,t-1} & & & \\ 0 & \alpha^u_{10} & \alpha^u_{11} & \cdots & \alpha^u_{1,t-1} & & & \\ \vdots & \vdots & \vdots & \cdots & \vdots & & & \\ 0 & \alpha^u_{r-1,0} & \alpha^u_{r-1,1} & \cdots & \alpha^u_{r-1,t-1} & & & \\ & & \gamma_{-p} & \gamma_{-(p-1)} & \cdots & \gamma_{p-1} & \gamma_p & \\ & & & \ddots & \ddots & \ddots & \ddots & \ddots \end{bmatrix} \tag{8}$$

With these limiting cases in mind, one can then construct what are here termed "cut-cell stencils" which vary smoothly between the uniform and degenerate cases. This is all that is needed to derive the cut-cell stencils for second order derivatives as given in tables 3-8 which give boundary closures suitable for Dirichlet and Neumann boundary conditions and achieve global accuracies of 4^{th}, 6^{th}, and 8^{th} order. The schemes are labeled according to the order of accuracy, boundary condition type and derivative order: $E4_{D2}$, $E4_{N2}$, $E6_{D2}$, $E6_{N2}$, $E8_{D2}$ and $E8_{N2}$. The coefficients for Neumann boundary conditions satisfy the equation:

$$f_i^{(2)} = \frac{1}{h}\alpha'_i f'_0 + \frac{1}{h^2}\sum_{j=0}^{t-1} \alpha^{ij} f_j \tag{9}$$

Cut-cell schemes for hyperbolic problems require the off-line optimization procedure of Ref. [33]. The optimization procedure results in a number of boundary schemes to choose from. Those used in this paper are in tables 1-2 and achieve global accuracies of 4^{th} ($E4_{D1}$) and 5^{th} ($E5_{D1}$) order, respectively.

IV. Results

The stability and accuracy of the schemes for parabolic and hyperbolic equations is demonstrated through a variety of tests and analysis. The asymptotic stability of the second derivative approximations given in tables 3-8 is explored through an eigenvalue analysis in section IV.A. The accuracy and stability of these schemes is demonstrated by solving the unsteady heat equation in section IV.B for a variety of embedded wall distances. The asymptotic stability of the conservative first derivative approximations given in tables 1-2 is also explored through an eigenvalue analysis presented in section IV.C. For the second test, in section IV.D, the compressible Euler equations are solved (without any numerical dissipation) with a moving (supersonic) isentropic vortex. The embedded wall distances are again varied at the supersonic inflow/outflow boundaries. In all tests considered, the schemes demonstrate the advertised order of accuracy and excellent stability properties over the whole range of $\psi \in [0,1]$

A. Asymptotic Stability: Eigenvalue Analysis for Parabolic terms

An asymptotically stable scheme is one for which the error does not grow unphysically with time [34]. To illustrate, consider the linear parabolic equation,

$$\frac{\partial u}{\partial t} = k\frac{\partial^2 u}{\partial x^2}, \qquad \text{for } x_0 \le x \le x_N, \text{and } t \ge 0, \tag{10}$$

with consistent initial and boundary conditions for $u = u(x,t)$,

$$u(x,0) = f(x) \qquad u(x_0,t) = a(t) \qquad u(x_N,t) = b(t). \tag{11}$$

Assuming a spatial discretization of $N+1$ points, the second derivative operator can be approximated as,

$$U'' = \boldsymbol{A}U, \tag{12}$$

where $\boldsymbol{A}$ is of dimension $(N+1)\times(N+1)$ and U, U'' are column vectors of length $N+1$. The fully discrete solution procedure involves solving Eq. 12 over the whole domain and updating U accordingly, except at the Dirichlet boundaries where $u(x)$ is imposed. Let the $N-1\times N-1$ submatrix of $\boldsymbol{A}$ which does not include the first or last row or column of $\boldsymbol{A}$, be denoted by $\boldsymbol{Q}$. With this notation, the semi-discrete system for $\hat{U} = [u_1, ..., u_{N-1}]^T$ can be written as,

$$\frac{\partial \hat{U}}{\partial t} = \boldsymbol{Q}\hat{U} + G, \tag{13}$$

where G is a column vector of length $N-1$ giving the appropriate weights of the stencils on the boundary data, $a(t)$ and $b(t)$. The stability of this semi-discrete system is governed by the eigenvalues, λ, of the spatial discretization matrix, $\boldsymbol{Q}$. Let the real and imaginary parts of an eigenvalue be given by $\mathrm{Re}(\lambda)$ and $\mathrm{Im}(\lambda)$, respectively. The semi-discrete system is then stable if [35],

$$\mathrm{Re}(\lambda) \le 0 \qquad \text{for all } \lambda. \tag{14}$$

The discretization matrix $\boldsymbol{Q}$ can be constructed for any scheme by consulting Tables 3-8. Figure 4 shows the maximum $\mathrm{Re}(\lambda)$, ω, of $\boldsymbol{Q}$ for schemes $E4$, $E6$, and $E8$ for $N+1 = 31, 61, 91$ as a function of embedded wall distances on the left and right sides of the domain, ψ_L and ψ_R, respectively. Note that ψ_L, ψ_R are sampled over the whole range of $\psi \in [0,1]$. The maximum real part of all eigenvalues is negative, satisfying the stability constraint given by Eq 14.

Similar plots can be shown when considering the case of Neumann boundary conditions. In that case, the boundary row/column is left in $\boldsymbol{Q}$ which results in a repeated row when $\psi = 0$, and thus a maximum eigenvalue of 0, which still satisfies the stability constraint (Eq. 14). This more challenging case will be explored in the next section.

B. Time Stability: Constant Coefficient Heat Equation

The stability of the discretizations for the 2^{nd} derivatives given in the appendix for Dirichlet and Neumann boundary conditions is demonstrated by considering the heat equation:

$$\frac{\partial T}{\partial t} = k\frac{\partial^2 T}{\partial x^2}, \tag{15}$$

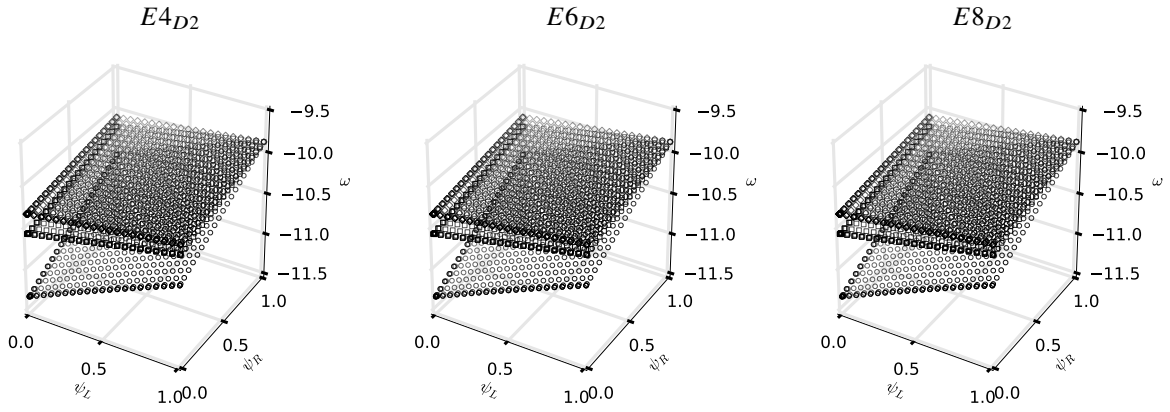

Fig. 4 Maximum $Re(\lambda)$, ω, as a function of embedded wall distances, ψ_L and ψ_R for $N = 31, 61,$ and 91 indicated by circle, square, and triangle markers, respectively. The maximum real part of all eigenvalues is negative.

on the domain $x \in [x_0, x_N]$, with initial and boundary conditions:

$$T(x,0) = \sum_{n=1}^{4} A_n \cos\left(\sigma_n (x - x_0)\right), \tag{16}$$

$$\left.\frac{\partial T}{\partial x}\right|_{x=x_0,\, t=t} = 0, \tag{17}$$

$$T(x_N, t) = 0, \tag{18}$$

where $\sigma_n = (n - 1/2)\pi/(x_N - x_0)$, $x_0 = h(1 - \psi_L)$, $x_N = 1 - h(1 - \psi_R)$, $A_1 = A_3 = 1$ and $A_2 = A_4 = 2$. The exact solution is:

$$T(x,t) = \sum_{n=1}^{4} A_n \exp\left(-\sigma_n^2 k t\right) \cos\left(\sigma_n (x - x_0)\right), \tag{19}$$

The combinations of left and right embedded wall distances to be considered are $(\psi_L, \psi_R) = (0,0)$, $(0.01, 0.5)$, $(0.2, 0.8)$, $(1.0, 0.1)$. Recall that $\psi = 0$ corresponds to the degenerate mesh case and $\psi = 1$ corresponds to the uniform mesh case. The test cases considered will use grid sizes of $N + 1 = 21, 41, 61, 81, 101$ and a thermal diffusivity of $k = 0.05$. The discretized heat equation is advanced in time using the standard 4^{th} order Runge-Kutta (RK4) method with the timestep constraint given by the well known parabolic stability constraint:

$$\Delta t = C \frac{h^2}{2k}\,. \tag{20}$$

Figure 5 (Left) shows the solution at times $t = 0, 1, 2, 100$ for the 8^{th} order $E8_{N2}/E8_{D2}$ schemes given in tables 5 and 8, respectively, for the case of $\psi_L = \psi_R = 0$ on the coarsest mesh with $N = 20$. In this challenging case, the mesh is degenerate on both sides but requires no reduction in the timestep compared to the uniform mesh case. Figure 5 (Right) shows the infinity norm, L_∞, of the error in temperature, T, on the coarsest mesh for a variety of combinations of (ψ_L, ψ_R) as a function of time, t. The simulations are stable and behave quantitatively similar for all combinations of (ψ_L, ψ_R) considered.

Grid convergence tests demonstrating the order of accuracy achieved using the second derivative approximations given the appendix, which were constructed based on the design principles, are given in Fig. 6. The simulations were run with a timestep restriction of $C = 0.2$ to minimize the temporal error. The error reported as L_∞ is the maximum error in temperature over the entire unsteady simulation for $t \in [0, 100]$. The schemes demonstrate the expected convergence properties for the different (ψ_L, ψ_R) combinations, even in the completely degenerate case of $\psi_L = \psi_R = 0$.

C. Asymptotic Stability: Eigenvalue Analysis for Hyperbolic terms

Similar to the eigenvalue analysis performed on the heat equation we now turn our attention to asymptotic stability for hyperbolic equations. An asymptotically stable scheme is one for which the error does not grow unphysically with

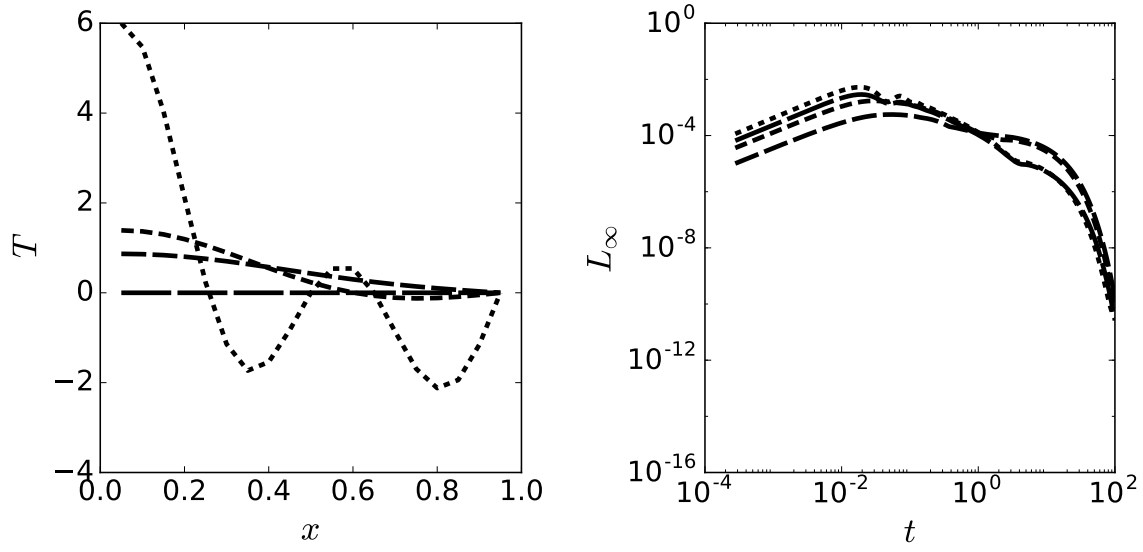

Fig. 5 (Left) Snapshots of solution using 8^{th} order $E8_{N2}/E8_{D2}$ schemes for $(\psi_L, \psi_R) = (0,0)$ at times $t = 0, 1, 2, 100$ corresponding to dashes of increasing length. (Right) Maximum error in temperature, L_∞, as a function of time for $N = 20$ with $(\psi_L, \psi_R) = (0,0), (0.01, 0.5), (0.2, 0.8), (1.0, 0.1)$ corresponding to dashes of increasing length.

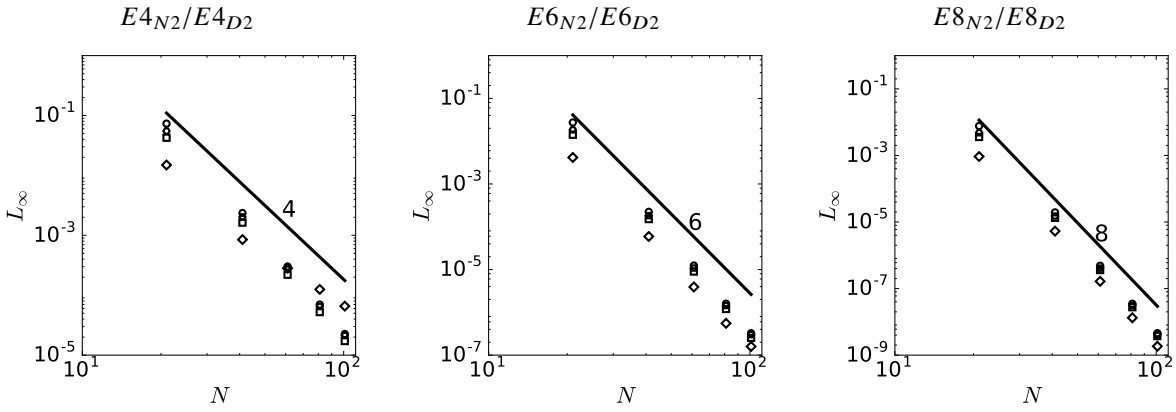

Fig. 6 Maximum error in Temperature, L_∞, as a function of grid resolution for the indicated scheme. Results for embedded wall distances of $(\psi_L, \psi_R) = (0,0), (0.01, 0.5), (0.2, 0.8), (1.0, 0.1)$ correspond to circles, squares, diamonds and hexagons, respectively. All schemes demonstrate their expected order of accuracy for the different ψ combinations considered.

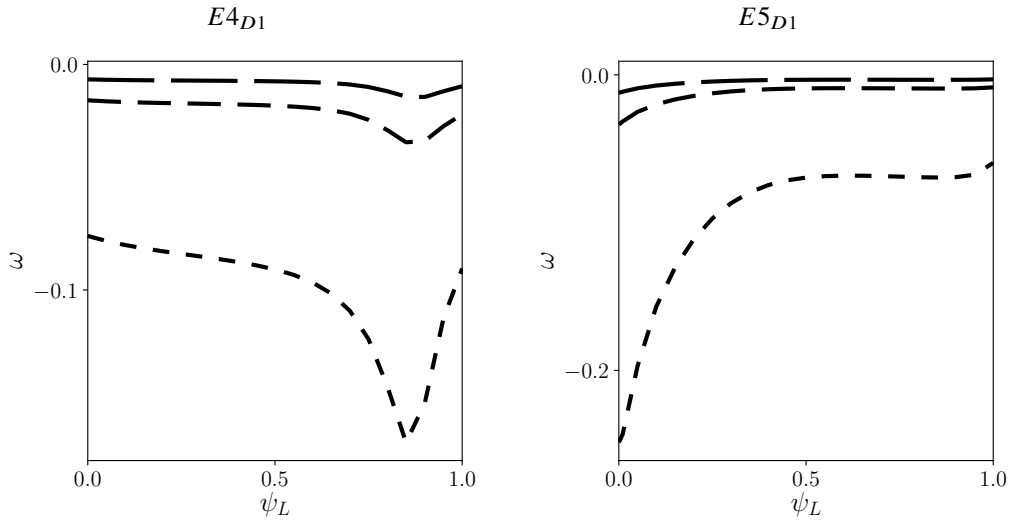

Fig. 7 Maximum $Re(\lambda)$, ω, as a function of embedded wall distance at the inflow, ψ_L, for $N = 30, 60,$ and 90 indicated by lines of increasing dash length, respectively. The maximum real part of all eigenvalues is negative.

time. To illustrate, consider the linear hyperbolic equation:

$$\frac{\partial u}{\partial t} + \frac{\partial u}{\partial x} = 0\,, \qquad \text{for } h(1-\psi_L) \le x \le 1, \text{and } t \ge 0\,, \tag{21}$$

with consistent initial and boundary conditions for $u = u(x,t)$

$$u(x,0) = f(x) \qquad u(h(1-\psi_L,t) = g(t)\,. \tag{22}$$

Assuming a spatial discretization of $N+1$ points, the first derivative operator can be approximated as:

$$U' = \boldsymbol{A}U\,, \tag{23}$$

where $\boldsymbol{A}$ is of dimension $(N+1)\times(N+1)$ and U, U' are column vectors of length $N+1$. The fully discrete solution procedure involves solving Eq. 23 over the whole domain and updating u accordingly, except at the boundary where $u(0,t) = g(t)$ is imposed. Let the $N \times N$ submatrix of $\boldsymbol{A}$ which does not include the first row or column of $\boldsymbol{A}$, be denoted by $\boldsymbol{Q}$. With this notation, the semi-discrete system for $\hat{U} = [u_1, u_2, ..., u_N]^T$ can be written as:

$$\frac{\partial \hat{U}}{\partial t} = \boldsymbol{Q}\hat{U} + G\,, \tag{24}$$

where G is a column vector of length N giving the appropriate weights of the stencils on the boundary point, u_0. The stability of this semi-discrete system is governed by the eigenvalues, λ, of the spatial discretization matrix, $\boldsymbol{Q}$. Let the real and imaginary parts of an eigenvalue be given by $\mathrm{Re}(\lambda)$ and $\mathrm{Im}(\lambda)$, respectively. The semi-discrete system is then stable if [35]

$$\mathrm{Re}(\lambda) \le 0 \qquad \text{for all } \lambda\,. \tag{25}$$

The discretization matrix $\boldsymbol{Q}$ can be constructed for any scheme by consulting Tables 1-2. Figure 7 shows the maximum real part, ω, of the eigenvalues of $\boldsymbol{Q}$ for schemes $E4_{D1}$, and $E5_{D1}$ for $N+1 = 31, 61, 91$. The real parts of all eigenvalues are negative, satisfying the stability constraint given by Eq 25. In all schemes, no eigenvalues with positive real parts are found, indicating asymptotic stability[34].

D. Nonlinear Test: Inviscid Vortex / Numerical Reflection

In this section we solve the two-dimensional compressible Euler equations to examine the transport of an inviscid vortex through a domain and it's numerical collision with a supersonic outflow boundary. This collision with the outflow

boundary generates very high frequency errors which propagate back into the domain with the potential to destabilize the simulation over long periods of time. The transport of an inviscid vortex through a periodic domain has been studied to quantify the impact of dissipation in upwinded schemes (e.g., Ref. [36]). The supersonic inflow/outflow case has been examined in Refs. [37] and [38] for relatively short times (1.5 flow through times based on the background streamwise velocity). In the present case, the conservative cut-cell schemes are used at the inflow/outflow boundaries and periodic boundary conditions are imposed in the cross-stream direction.

The notations from Ref. [38] are adopted here to describe the analytic solution for a vortex of nondimensional circulation, ϵ, propagating in the x direction. The solutions are repeated below for convenience:

$$\frac{\rho}{\rho_\infty} = \left(1 - \frac{(\gamma-1)}{2}\eta^2\right)^{1/(\gamma-1)}, \tag{26}$$

$$\frac{u}{a_\infty} = M_\infty + Ky\eta, \tag{27}$$

$$\frac{v}{a_\infty} = -Kx\eta, \tag{28}$$

$$\frac{p}{p_\infty} = \left(\frac{\rho}{\rho_\infty}\right)^\gamma, \tag{29}$$

where $\eta = \frac{\epsilon}{2\pi}\exp((1-K^2(x^2+y^2))/2)$, M_∞ is the free stream Mach number, and $\gamma = c_p/c_v = 1.4$. As with the previous tests, time integration is carried out using a standard RK4 method. The tests were run on a computational domain of $x \in [h(1-\psi_L), 20 - h(1-\psi_R)]$, $y \in [0, 10]$ with $(x_c, y_c) = (10, 5)$, $\epsilon = 1.5$ and $M = 2.0$

All schemes were tested on four different grid resolutions, $N_x \times N_y = 51 \times 26$, 101×51, 201×101, and 401×201 with two different timesteps, $C = 0.8, 0.1$ until a time of $t = 1000$ (50 flow through times).

To illustrate the performance of the conservative cut-cell schemes, early time results with $E5_{D1}$ are shown in Fig. 8, which depicts contours of the pressure at times $t = 0, 5$, and 10 for the different grid resolutions on degenerate meshes with $\psi_L = \psi_R = 0$. Half of the vortex has propagated through the outflow boundary by a time of $t = 10$ and the presence of a degenerate mesh at the outflow does not have a noticeable impact on the quality of the solution. Wireframe plots of the error in pressure, P_ϵ, are shown for the coarsest mesh with $\psi_L = \psi_R = 0$ in Fig. 9 at the times of $t = 10$ and $t = 25$. High-frequency errors appear, especially at the outflow boundary, as the vortex exits the domain around $t = 10$. At the later time of $t = 25$, the point-to-point oscillations in P_ϵ are more pronounced, especially at the outflow boundary where $\psi_R = 0$. However, all the optimized conservative schemes developed in section III are stable to these kinds of perturbations. The evolution of the infinity norm of the pressure error, $L_\infty(P_\epsilon)$ over time using the conservative 5^{th} order cut-cell scheme $E5_{D1}$ is shown in Fig. 10 for the degenerate mesh case with $\psi_L = \psi_R = 0$. There is a sharp increase in error as the vortex impacts the outflow around time $t = 10$. After this, the error exhibits complex behavior as high frequency error waves bounce back and forth between the inflow and outflow boundaries before ultimately decaying. The magnitude of the peak error does not appear to be affected by the size of the timestep. The size of the timestep impacts how accurately the evolution of the vortex is captured for $t \leq 10$. The late-time results are not appreciably impacted by the timestep constraint.

Figure 11 shows the evolution of $L_\infty(P_\epsilon)$ for the rest of the schemes considered in the paper for the less dissipative $C = 0.1$. The optimized conservative cut-cell schemes $E4_{D1}$, and $E5_{D1}$ display stable, converging behavior for this challenging inviscid test problem. The schemes all exhibit very similar behavior for the larger timestep, demonstrating excellent stability properties over the range $\psi \in [0, 1]$ for this very challenging non-linear, inviscid, hyperbolic test case.

V. Conclusions

The numerical challenges facing cut-cell methods stem from the highly irregular grids which naturally arise near the embedded boundaries of a non-Cartesian object embedded in a Cartesian mesh. This paper has focused exclusively on the stability issues that result from approximating derivatives on this irregular, and at times, degenerate mesh. This has been termed the “small-cell problem" in the literature. Previous attempts to solve this classic problem have employed either geometric manipulation algorithms to redistribute the irregularities or some kind of dynamic correction procedure which often results in numerical source terms being added to the governing equations. These approaches have been largely limited to 2^{nd} order accuracy for unsteady problems.

In this paper, a fundamentally different approach has been taken. This method is based on the intuitive design principles that a degenerate mesh ought to yield the same solution as the equivalent uniform mesh and that the Taylor

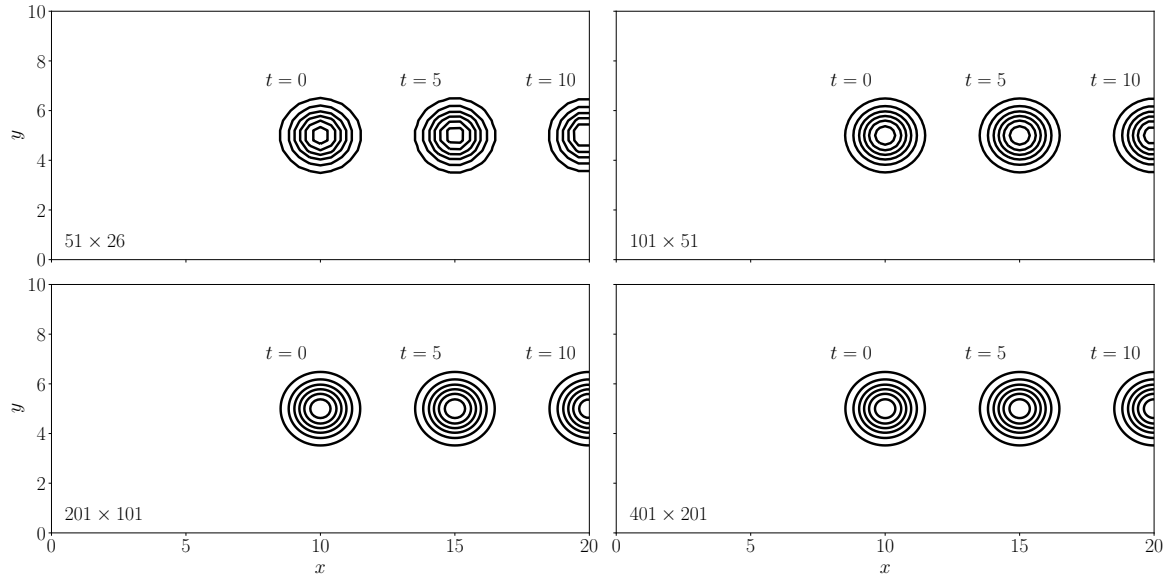

Fig. 8 Pressure contours of the solution computed with the 5^{th} order conservative cut-cell scheme $E5_{D1}$ and embedded wall distances $(\psi_L, \psi_R) = (0, 0)$ at times $t = 0, 5, 10$ as the vortex moves from left to right at the indicated resolutions. The pressure contours are drawn at the same values for all times and grids. The contours range from 0.12 at the outer edge of the vortex to 0.18 in the interior of the vortex.

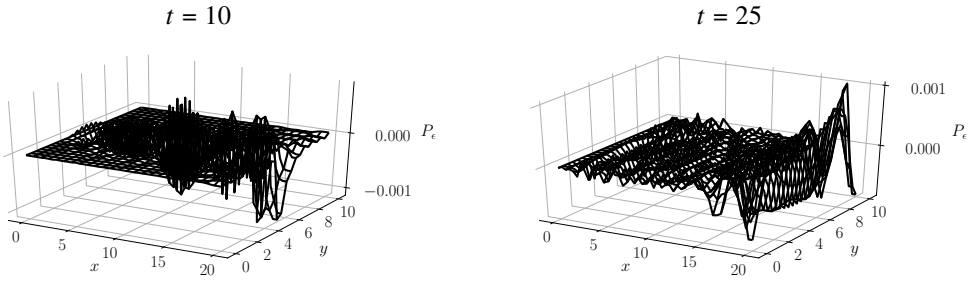

Fig. 9 Wireframe plot of pressure error, P_ϵ, at indicated times for the solution computed with the conservative 5^{th} order $E5_{D1}$ cut-cell scheme at the coarsest resolution of 51×26 points on a degenerate mesh with $\psi_L = \psi_R = 0$.

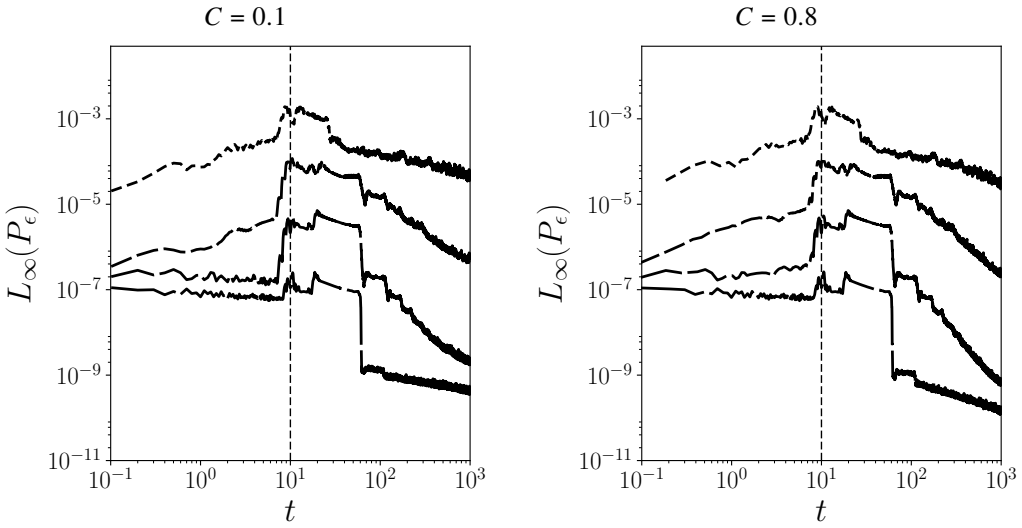

Fig. 10 Evolution of infinity norm of pressure error, $L_\infty(P_\epsilon)$ for the inviscid vortex simulation for the indicated time constraints with the 5^{th} order cut-cell scheme $E5_{D1}$ for the degenerate mesh case (i.e. $\psi_L = \psi_R = 0$). The short, medium, long and longer dashed lines correspond to grids with $N_x = 51, 101, 201$ and 401, respectively. The vertical dashed line at $t = 10$ is when the half the vortex has left the domain through the outflow.

series, which forms the foundation of finite differences, ought not be violated in the process. These two principles are all that is needed to construct the stable 4^{th}, 6^{th} and 8^{th} order approximations to parabolic equations.

The construction of stable and conservative approximations to hyperbolic problems requires that these two design principles be supplemented with discrete conservation constraints and a novel non-linear optimization strategy. This process produced stable and conservative approximations of 4^{th} and 5^{th} order.

The stability and accuracy of the schemes for parabolic and hyperbolic equations is demonstrated through a variety of tests and analysis. Asymptotic stability of is explored through an eigenvalue analysis in which all schemes yielded stable eigenvalues. The accuracy and stability of the second derivative approximations was demonstrated by solving the unsteady heat equation for a variety of embedded wall distances. The accuracy and long-time stability of the conservative cut-cell discretizations was assessed by solving the compressible Euler equations (without any numerical dissipation) for a moving (supersonic) isentropic vortex. The embedded wall distances are again varied at the supersonic inflow/outflow boundaries. In all tests considered, the schemes demonstrate the advertised order of accuracy and excellent stability properties over the whole range of geometries, from uniform to degenerate meshes.

Appendix

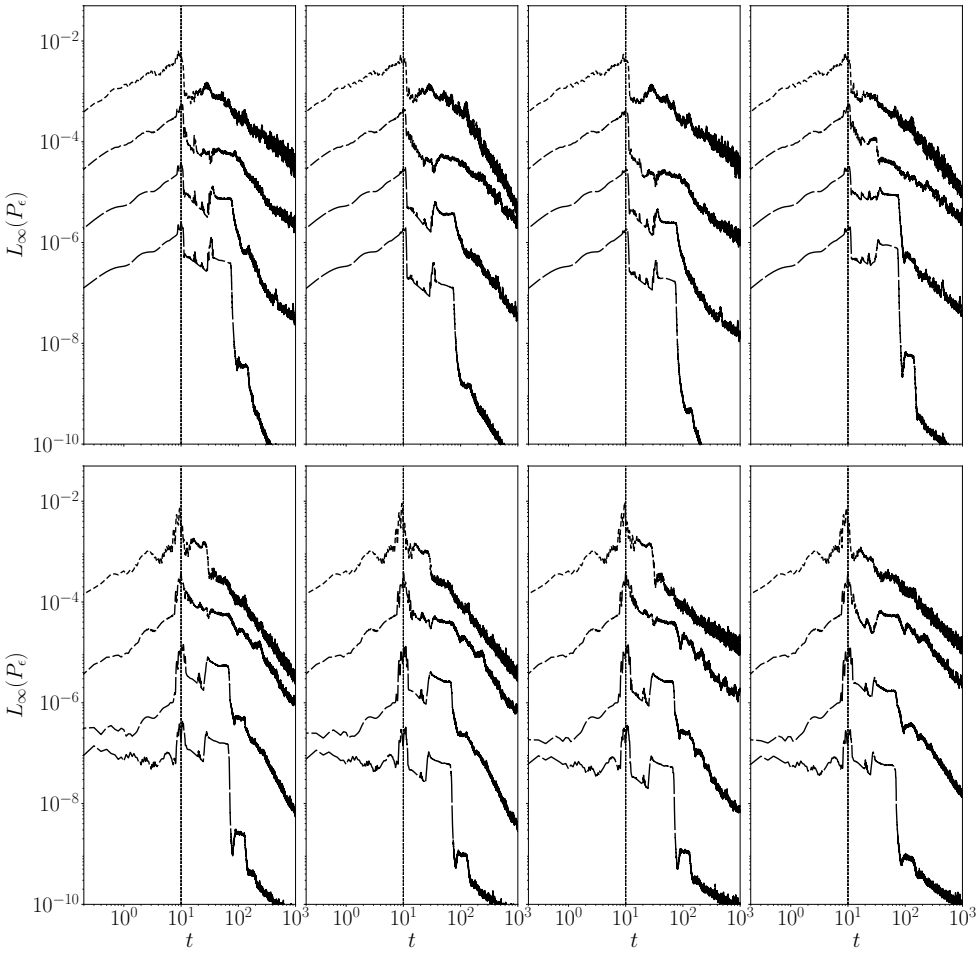

Fig. 11 L_∞ **norm of error in Pressure as a function of time,** t**, for the indicated conservative cut-cell scheme. The short, medium, long and longer dashed lines correspond to grids with** $N_x = 51, 101, 201$ **and** 401**, respectively. The columns (from left to right) correspond to embedded wall distances of** $(\psi_L, \psi_R) = (0,0), (0.01, 0.5), (0.2, 0.8)$ **and** $(1.0, 0.1)$**, respectively. The top and bottoms rows corresponds to** $E4_{D1}$ **and** $E5_{D1}$**, respectively. Results are for the case with constant CFL** $= 0.1$**. The vertical dashed line at** $t = 10$ **is when the half the vortex has left the domain through the outflow.**

$$\alpha_{00} = 2.137265266999951(-0.2339438195717479\psi^2 - 2.766056180428252\psi - 1.0)/$$
$$(0.16666666666666667\psi^3 + \psi^2 + 1.833333333333333\psi + 1.0)$$
$$\alpha_{01} = 4.2157277346664 69\psi$$
$$\alpha_{02} = 4.215727734666469(-2.953491288177581\psi^2 + 0.3767331049251927\psi + 1.0)/(\psi + 1.0)$$
$$\alpha_{03} = 4.431455469332938(1.889368567040984\psi^2 - 0.1902478927073298\psi - 1.0)/(0.6666666666666666\psi + 1.333333333333333)$$
$$\alpha_{04} = 2.313761767833161(-1.0\psi^2 - 0.2669651258341296\psi + 1.004248421035909)/(0.5\psi + 1.5)$$
$$\alpha_{05} = 0.3039319336666173(\psi - 1.0)$$
$$\alpha_{10} = 1.550045434342208(0.6211595998107364\psi - 1.378840400189264)/(0.16666666666666667\psi^3 + \psi^2 + 1.833333333333333\psi + 1.0)$$
$$\alpha_{11} = 0.6588936680178477(-1.0\psi)$$
$$\alpha_{12} = 3.411795800999852(0.4902840521395548\psi^2 - 1.0\psi + 1.235633074356624)/(\psi + 1.0)$$
$$\alpha_{13} = 4.431455469332938(-0.160200970903432\psi^2 + 1.013269409958052\psi - 1.0)/(0.6666666666666666\psi + 1.333333333333333)$$
$$\alpha_{14} = 2.117693701499778(-0.05971168842852386\psi^2 - 1.0\psi + 1.097227422622123)/(0.5\psi + 1.5)$$
$$\alpha_{15} = 0.3039319336666173(\psi - 1.0)$$
$$\alpha_{20} = 0.2057238599777199(\psi)$$
$$\alpha_{21} = 0.2315692382960836(-0.1480650463272977\psi^4 - 0.888390277963786\psi^3 - 1.628715509600274\psi^2 - 1.0\psi - 1.267914160314605)$$
$$\alpha_{22} = 0.5143096499442996(0.2\psi^4 + \psi^3 + 1.2\psi^2 + 0.2010102538123699\psi - 1.281122506819008)$$
$$\alpha_{23} = 0.3085857899665798(-0.3333333333333333\psi^4 - 1.3333333333333333\psi^3 - 1.0\psi^2 - 0.5025256345309248\psi + 4.01295374670 65)$$
$$\alpha_{24} = 0.1028619299888599(0.3333333333333333\psi^4 + \psi^3 + 0.6666666666666666\psi^2 + 1.005051269061 85\psi - 3.165022615459119)$$
$$\alpha_{25} = 0.0327843976614128(1.21165614859584 - 0.788343851404 16\psi)$$
$$\alpha_{30} = 0.006886757691141544(\psi)$$
$$\alpha_{31} = 0.0126257224337595(-0.09090909090909091\psi^4 - 0.5454545454545454\psi^3 - 1.0\psi^2 - 12.41398546799121\psi + 16.29402682159729)$$
$$\alpha_{32} = 0.0206602730734246 3(0.1666666666666667\psi^4 + 0.8333333333333334\psi^3 + \psi^2 + 28.34023866629391\psi - 55.29214112990228)$$
$$\alpha_{33} = 0.0137735153822830 9(-0.25\psi^4 - 1.0\psi^3 - 0.75\psi^2 - 61.24656520784404\psi + 49.2852395543921)$$
$$\alpha_{34} = 0.0034433788455707 72(0.3333333333333333\psi^4 + \psi^3 + 0.6666666666666666\psi^2 + 149.8896576672254\psi + 75.6154939328352)$$
$$\alpha_{35} = 0.0553957919066931 2(-1.702956472559219\psi - 0.2970435274407811)$$
$$\alpha_{36} = 0.0138780386860982(1.0 - 1.0\psi)$$
$$\alpha_{41} = 0.6051176652999009(-0.02844144743770986\psi^9 - 0.3433338666178695\psi^8 - 1.507604661826747\psi^7$$
$$- 2.328524394244007\psi^6 + 1.3725765254480 05\psi^5 + 4.808784885445197\psi^4 - 0.4961720408348927\psi^3 + 0.6274234745511995\psi^2$$
$$- 2.155036942722248\psi + 0.0503284682382769)/(0.04097006780909419\psi^8 + 0.3474349240783006\psi^7 + \psi^6 + 0.6696760672003487\psi^5$$
$$+ 0.4616970115779694\psi^4 + 5.797740516195518\psi^3 + 5.1265976677566 56\psi^2 + 14.61909118122837\psi + 4.42220367904627)$$
$$\alpha_{42} = 2.099413220951042(0.0323480366127683\psi^9 + 0.3951547271782681\psi^8 + 1.756880603065215\psi^7 + 2.784396834038143\psi^6$$
$$- 1.467625983272 52\psi^5 - 5.696789300395109\psi^4 + 0.5323740167274801\psi^3 - 0.2563671798036345\psi^2 + 3.149421957242327\psi$$
$$+ 0.0596702044727419 6)/(0.04097006780909419\psi^8 + 0.3474349240783006\psi^7 + \psi^6 + 0.6696760672003487\psi^5$$
$$+ 0.4616970115779694\psi^4 + 5.797740516195518\psi^3 + 5.1265976677566 56\psi^2 + 14.61909118122837\psi + 4.42220367904627)$$
$$\alpha_{43} = 3.598266444661811(-0.0276642549307946 1\psi^9 - 0.3486276141407602\psi^8 - 1.597075442013657\psi^7 - 2.675015631552434\psi^6$$
$$+ 1.054864960160624\psi^5 + 5.165529999175711\psi^4 - 0.9451350398393763\psi^3 - 0.9317357774291054\psi^2 - 5.080300145161113\psi$$
$$- 0.6335561984437911)/(0.04097006780909419\psi^8 + 0.3474349240783006\psi^7 + \psi^6 + 0.6696760672003487\psi^5$$
$$+ 0.4616970115779694\psi^4 + 5.797740516195518\psi^3 + 5.1265976677566 56\psi^2 + 14.61909118122837\psi + 4.42220367904627)$$
$$\alpha_{44} = 2.204016820429829(0.0287034692332569\psi^9 + 0.3638472965788683\psi^8 + 1.683847616138181\psi^7 + 2.900600482940353\psi^6$$
$$- 1.002874532890264\psi^5 - 6.257993753527582\psi^4 - 0.9971254671097356\psi^3 + 0.8169982328399389\psi^2 + 2.84982603362651\psi$$
$$- 0.3858293778295254)/(0.04097006780909419\psi^8 + 0.3474349240783006\psi^7 + \psi^6 + 0.6696760672003487\psi^5$$
$$+ 0.4616970115779694\psi^4 + 5.797740516195518\psi^3 + 5.1265976677566 56\psi^2 + 14.61909118122837\psi + 4.42220367904627)$$
$$\alpha_{45} = 1.415717130426091(-0.0095296218346 2712\psi^9 - 0.1137524906454 85\psi^8 - 0.5100350386640293\psi^7$$
$$- 0.8807758277660492\psi^6 + 0.3784195928640869\psi^5 + 3.286776550421 83\psi^4 + 4.118538370488724\psi^3 + 1.119224172233951\psi^2$$
$$+ 5.461615519603 04\psi + 2.447024382165182)/(0.04097006780909419\psi^8 + 0.3474349240783006\psi^7 + \psi^6 + 0.6696760672003487\psi^5$$
$$+ 0.4616970115779694\psi^4 + 5.797740516195518\psi^3 + 5.1265976677566 56\psi^2 + 14.61909118122837\psi + 4.42220367904627)$$
$$\alpha_{46} = 0.1277608302575437(-0.0072776088453626 57\psi^9 - 0.0646899147696637 5\psi^8 - 0.1455869343840247\psi^7$$
$$+ 0.3350626232292 34\psi^6 + 1.013731198183201\psi^5 - 3.110041975388113\psi^4 - 8.215247994684342\psi^3 + 0.9862688018167989\psi^2$$
$$- 8.146321474631966\psi - 3.834844752959727)/(0.04097006780909419\psi^8 + 0.3474349240783006\psi^7 + \psi^6 + 0.6696760672003487\psi^5$$
$$+ 0.4616970115779694\psi^4 + 5.797740516195518\psi^3 + 5.1265976677566 56\psi^2 + 14.61909118122837\psi + 4.42220367904627)$$

Table 1 Scheme $E4_{D1}$: 3^{rd} order conservative cut-cell boundary closures for first derivatives with 4^{th} order interior scheme. 4^{th} order accuracy overall.

$$\alpha_{00} = 2.000598634247677(-0.0833083977033412\psi^3 - 0.6248129827750589\psi^2 - 4.792626688421364\psi - 1.375187017224941)/(0.04166666666666666\psi^4 + 0.4166666666666667\psi^3 + 1.458333333333333\psi^2 + 2.083333333333333\psi + 1.0)$$

$$\alpha_{01} = 7.339319675810099(\psi)$$

$$\alpha_{02} = 4.500598634247677(0.03703211066154687\psi^3 - 6.338077432930364\psi^2 + 0.3692570095095927\psi + 1.630742990490407)/(\psi + 1.0)$$

$$\alpha_{03} = 6.847700555277571(-0.04867814102595812\psi^3 + 4.157831128932159\psi^2 + 0.1154473148097765\psi - 1.884552685190223)/(0.6666666666666666\psi + 1.333333333333333)$$

$$\alpha_{04} = 8.266163124687267(0.03024377770302691\psi^3 - 1.806428318902936\psi^2 - 0.5461260749212506\psi + 1.453873925078749)/(0.5\psi + 1.5)$$

$$\alpha_{05} = 3.572653009143433(-0.0186602691322408\psi^3 + 1.008860966166829\psi^2 + 0.9911390338331713\psi - 1.60746410765289)/(0.4\psi + 1.6)$$

$$\alpha_{06} = 0.6678639351620198(1.0 - 1.0\psi)$$

$$\alpha_{10} = 1.836385745432242(0.501841306850383\psi - 1.498158693149617)/(0.04166666666666666\psi^4 + 0.4166666666666667\psi^3 + 1.458333333333333\psi^2 + 2.083333333333333\psi + 1.0)$$

$$\alpha_{11} = 0.2537102872071113(-1.0\psi)$$

$$\alpha_{12} = 7.004789073981413(0.04953428433059284\psi^2 - 1.0\psi + 1.047757412578098)/(\psi + 1.0)$$

$$\alpha_{13} = 12.90485246882693(0.0593675399844833\psi^2 + 1.042802724084002\psi - 1.0)/(0.6666666666666666\psi + 1.333333333333333)$$

$$\alpha_{14} = 11.51436722194424(-0.1299395096779972\psi^2 - 1.0\psi + 1.043735951423045)/(0.5\psi + 1.5)$$

$$\alpha_{15} = 5.00766251837026(0.193123673536037\psi^2 + \psi - 1.14682478306569)/(0.4\psi + 1.6)$$

$$\alpha_{16} = 0.6678639351620198(1.0 - 1.0\psi)$$

$$\alpha_{20} = 0.07023737412138484(\psi)$$

$$\alpha_{21} = 0.074058369515439 56(-0.03951690098237415\psi^5 - 0.3951690098237415\psi^4 - 1.383091534383095\psi^3 - 1.975845049118708\psi^2 + 0.6169084656169047\psi - 4.941029779881355)$$

$$\alpha_{22} = 0.2673298918463253(0.04378945032813665\psi^5 + 0.3941050529532298\psi^4 + 1.138525708531553\psi^3 + 1.050946807875279\psi^2 - 2.168193919965443\psi - 0.9490531921247204)$$

$$\alpha_{23} = 0.2721698247203662(-0.06451612903225806\psi^5 - 0.5161290322580645\psi^4 - 1.225806451612903\psi^3 - 0.7741935483870968\psi^2 + 4.259274860626012\psi + 1.251990032685125)$$

$$\alpha_{24} = 0.1287685192225389(0.09090909090909091\psi^5 + 0.6363636363636364\psi^4 + 1.272727272727273\psi^3 + 0.7272727272727273\psi^2 - 9.002558228141345\psi + 5.119621598763043)$$

$$\alpha_{25} = 0.02487573666799046(-0.1176470588235294\psi^5 - 0.7058823529411765\psi^4 - 1.294117647058824\psi^3 - 0.7058823529411765\psi^2 + 23.30073894342465\psi - 19.95075440043161)$$

$$\alpha_{26} = 0.1159246092252444(1.0 - 1.0\psi)$$

$$\alpha_{30} = 0.09001252151243926(\psi)$$

$$\alpha_{31} = 0.07705689771160515(-0.04867210906571602\psi^5 - 0.4867210906571602\psi^4 - 1.703523817300061\psi^3 - 2.433605453285801\psi^2 - 1.088499846123357\psi + 0.9115001538766431)$$

$$\alpha_{32} = 0.2475344341592 08(0.06060606060606061\psi^5 + 0.5454545454545454\psi^4 + 1.575757575757576\psi^3 + 1.454545454545455\psi^2 - 0.1239443762936678\psi - 2.428699961073924)$$

$$\alpha_{33} = 0.1554923175721817(-0.1447218147460149\psi^5 - 1.157774517968 12\psi^4 - 2.749714480174284\psi^3 - 1.736661776952179\psi^2 + 0.3946240114252162\psi - 0.8422254820318803)$$

$$\alpha_{34} = 0.1125156518905491(0.13333333333333333\psi^5 + 0.9333333333333333\psi^4 + 1.866666666666667\psi^3 + 1.066666666666667\psi^2 - 0.5453552556921382\psi + 7.089024907948381)$$

$$\alpha_{35} = 0.0265918157155894(-0.1410404528144437\psi^5 - 0.846242716886662\psi^4 - 1.551444980958 88\psi^3 - 0.846242716886662\psi^2 + 1.153757283113338\psi - 5.596200386791 73)$$

$$\alpha_{36} = 0.00961602971128115(1.361888388987072 - 0.6381116110129285\psi)$$

$$\alpha_{40} = 0.2749814532256096(\psi)$$

$$\alpha_{41} = 0.2535021626275586(-0.04519709193921289\psi^5 - 0.4519709193921289\psi^4 - 1.581898217872451\psi^3 - 2.259854596960645\psi^2 - 1.548029080607871\psi + 0.3550759511455696)$$

$$\alpha_{42} = 0.495122929175093(0.09256336053881492\psi^5 + 0.8330702448493343\psi^4 + 2.406647374009188\psi^3 + 2.221520652931558\psi^2 + 1.166929755150666\psi - 0.754740108386392)$$

$$\alpha_{43} = 0.6874536330640 24(-0.1\psi^5 - 0.8\psi^4 - 1.9\psi^3 - 1.2\psi^2 - 1.639615154483195\psi + 0.3902195443622246)$$

$$\alpha_{44} = 0.5041326642469509(0.09090909090909091\psi^5 + 0.6363636363636364\psi^4 + 1.272727272727273\psi^3 + 0.7272727272727273\psi^2 + 2.141988014161427\psi - 1.923548847179475)$$

Table 2 Scheme $E5_{D1}$: 4^{th} order conservative cut-cell boundary closures for first derivatives with 6^{th} order interior scheme. 5^{th} order accuracy overall.

$$\alpha_{45} = 0.09738926468407007(-0.1176470588235294\psi^5 - 0.7058823529411765\psi^4 - 1.294117647058824\psi^3$$
$$- 0.7058823529411765\psi^2 - 5.058152901842649\psi + 12.18130014730728)$$
$$\alpha_{46} = 0.139139572979608(0.504054990286973\psi - 1.495945009713027)$$
$$\alpha_{47} = 0.008211256541874067(1.152400248872721\psi + 0.847599751127279)$$
$$\alpha_{51} = 2.608682616255373(1.34517787641921e - 6\psi^{12} - 0.0013132401445607\psi^{11} - 0.02614756238538718\psi^{10}$$
$$- 0.2179029849761506\psi^9 - 1.0\psi^8 - 2.783193300776836\psi^7 - 4.480120919730242\psi^6 - 2.010750879182381\psi^5 + 4.800858937652098\psi^4$$
$$+ 3.849020488159466\psi^3 + 0.1427210447217529\psi^2 + 0.6620224400476042\psi + 1.064804631436759)/(1.038864132242691e - 4\psi^{11}$$
$$- 0.0011918823723293362\psi^{10} - 0.03050253249225655\psi^9 - 0.199530842703032\psi^8 - 0.5086095010057331\psi^7$$
$$+ 1.0656465912780 71\psi^6 + 11.53066235398025\psi^5 + 30.27954611369828\psi^4 + 29.74730137653994\psi^3 - 0.9343534087219293\psi^2$$
$$+ 28.09471177228562\psi + 10.10154430109247)$$
$$\alpha_{52} = 13.072017899110 33(-1.295653267319673e - 6\psi^{12} + 0.0013109828056414 33\psi^{11} + 0.02611899687189496\psi^{10}$$
$$+ 0.2178122318864798\psi^9 + \psi^8 + 2.781708220717725\psi^7 + 4.460509943972 09\psi^6 + 1.936805205324264\psi^5 - 4.909037082011304\psi^4$$
$$- 3.878021131031275\psi^3 - 0.02440724506387583\psi^2 - 0.6682827445135813\psi - 1.083675072975674)/(1.038864132242691e - 4\psi^{11}$$
$$- 0.0011918823723293362\psi^{10} - 0.03050253249225655\psi^9 - 0.199530842703032\psi^8 - 0.5086095010057331\psi^7$$
$$+ 1.0656465912780 71\psi^6 + 11.53066235398025\psi^5 + 30.27954611369828\psi^4 + 29.74730137653994\psi^3 - 0.9343534087219293\psi^2$$
$$+ 28.09471177228562\psi + 10.10154430109247)$$
$$\alpha_{53} = 26.246605793733 04(1.220991454258029e - 6\psi^{12} - 0.0013064506523612 04\psi^{11} - 0.02606351961 10689\psi^{10}$$
$$- 0.2176347280049593\psi^9 - 1.0\psi^8 - 2.779418517580411\psi^7 - 4.425858401847932\psi^6 - 1.793124589870234\psi^5 + 5.150881221023 68\psi^4$$
$$+ 3.996089353560786\psi^3 - 0.1612144894588679\psi^2 + 0.7445485308976144\psi + 1.136868615591765)/(1.038864132242691e - 4\psi^{11}$$
$$- 0.0011918823723293362\psi^{10} - 0.03050253249225655\psi^9 - 0.199530842703032\psi^8 - 0.5086095010057331\psi^7$$
$$+ 1.0656465912780 71\psi^6 + 11.53066235398025\psi^5 + 30.27954611369828\psi^4 + 29.74730137653994\psi^3 - 0.9343534087219293\psi^2$$
$$+ 28.09471177228562\psi + 10.10154430109247)$$
$$\alpha_{54} = 34.141201980020 02(-8.494821404344135e - 7\psi^{12} + 0.0010037602066728 12\psi^{11} + 0.02011197135718118\psi^{10}$$
$$+ 0.1685705092100826\psi^9 + 0.7763796593081604\psi^8 + 2.154492036677997\psi^7 + 3.367979825364955\psi^6 + 1.061901723854405\psi^5$$
$$- 4.666134072954 28\psi^4 - 3.599254063792021\psi^3 + 0.3850200264905853\psi^2 - 1.0\psi - 1.067730579888789)/(1.038864132242691e - 4\psi^{11}$$
$$- 0.0011918823723293362\psi^{10} - 0.03050253249225655\psi^9 - 0.199530842703032\psi^8 - 0.5086095010057331\psi^7$$
$$+ 1.0656465912780 71\psi^6 + 11.53066235398025\psi^5 + 30.27954611369828\psi^4 + 29.74730137653994\psi^3 - 0.9343534087219293\psi^2$$
$$+ 28.09471177228562\psi + 10.10154430109247)$$
$$\alpha_{55} = 15.001092144891 91(7.637197688277408e - 7\psi^{12} - 0.0011472300628310 26\psi^{11} - 0.02298491519 6993\psi^{10}$$
$$- 0.1928303691843228\psi^9 - 0.888651362761483\psi^8 - 2.461602932333694\psi^7 - 3.824284054493126\psi^6 - 1.219462949997191\psi^5$$
$$+ 4.990904707010992\psi^4 + 3.372926708651 82\psi^3 - 1.013514278911959\psi^2 + 0.2606459135590182\psi + 1.0)/(1.038864132242691e - 4\psi^{11}$$
$$- 0.0011918823723293362\psi^{10} - 0.03050253249225655\psi^9 - 0.199530842703032\psi^8 - 0.5086095010057331\psi^7$$
$$+ 1.0656465912780 71\psi^6 + 11.53066235398025\psi^5 + 30.27954611369828\psi^4 + 29.74730137653994\psi^3 - 0.9343534087219293\psi^2$$
$$+ 28.09471177228562\psi + 10.10154430109247)$$
$$\alpha_{56} = 4.229886509808709(-1.098379586482297e - 7\psi^{12} + 8.358071637267053e - 4\psi^{11} + 0.01638076809368214\psi^{10}$$
$$+ 0.1355446421166605\psi^9 + 0.6193938904513088\psi^8 + 1.712761973091922\psi^7 + 2.830105297491848\psi^6 + 2.256384630086162\psi^5$$
$$+ 0.7494724411042339\psi^4 + 2.799940017405 85\psi^3 + 1.975841773259572\psi^2 + 5.255866645713352\psi + 1.0)/(1.038864132242691e - 4\psi^{11}$$
$$- 0.0011918823723293362\psi^{10} - 0.03050253249225655\psi^9 - 0.199530842703032\psi^8 - 0.5086095010057331\psi^7$$
$$+ 1.0656465912780 71\psi^6 + 11.53066235398025\psi^5 + 30.27954611369828\psi^4 + 29.74730137653994\psi^3 - 0.9343534087219293\psi^2$$
$$+ 28.09471177228562\psi + 10.10154430109247)$$
$$\alpha_{57} = 0.06779665579197063(-8.981387081324486e - 6\psi^{12} - 2.465346005125762e - 4\psi^{11} - 0.00405940117419 1486\psi^{10}$$
$$- 0.03694682932493294\psi^9 - 0.1861021961842513\psi^8 - 0.4279436806706403\psi^7 - 1.0\psi^6 - 9.298503596985888\psi^5$$
$$- 38.41362459762024\psi^4 - 62.52700015570908\psi^3 - 33.70021890818694\psi^2 - 75.32587984998747\psi$$
$$- 20.56334147047918)/(1.038864132242691e - 4\psi^{11} - 0.0011918823723293362\psi^{10} - 0.03050253249225655\psi^9$$
$$- 0.199530842703032\psi^8 - 0.5086095010057331\psi^7 + 1.0656465912780 71\psi^6 + 11.53066235398025\psi^5 + 30.27954611369828\psi^4$$
$$+ 29.74730137653994\psi^3 - 0.9343534087219293\psi^2 + 28.09471177228562\psi + 10.10154430109247)$$
$$\alpha_{58} = 0.1640214656276631(7.802136460261094e - 4\psi^8 + 0.01365373880545692\psi^7 + 0.1307082047146061\psi^6$$
$$+ 0.7055429308112386\psi^5 + 1.990537157507802\psi^4 + 2.742783903170397\psi^3 + \psi^2 + 3.495138395156572\psi$$
$$+ 1.011408737362079)/(1.038864132242691e - 4\psi^{11} - 0.0011918823723293362\psi^{10} - 0.03050253249225655\psi^9$$
$$- 0.199530842703032\psi^8 - 0.5086095010057331\psi^7 + 1.0656465912780 71\psi^6 + 11.53066235398025\psi^5 + 30.27954611369828\psi^4$$
$$+ 29.74730137653994\psi^3 - 0.9343534087219293\psi^2 + 28.09471177228562\psi + 10.10154430109247)$$

Table 2 (Continued) Scheme $E5_{D1}$: 4^{th} order conservative cut-cell boundary closures for first derivatives with 6^{th} order interior scheme. 5^{th} order accuracy overall.

$$\alpha_{00} = (36\psi + 12) / \left(\psi^3 + 6\psi^2 + 11\psi + 6\right) \qquad \alpha_{10} = 12 / \left(\psi^2 + 5\psi + 6\right) \qquad \alpha_{20} = -\psi / 12$$

$$\alpha_{01} = -5\psi \qquad \alpha_{11} = -2\psi \qquad \alpha_{21} = \left(\psi^4 + 6\psi^3 + 11\psi^2 + 6\psi + 72\right) / 72$$

$$\alpha_{02} = \left(15\psi^2 - 2\psi - 5\right) / (\psi + 1) \qquad \alpha_{12} = 6\psi - 5 \qquad \alpha_{22} = -\left(\psi^4 + 5\psi^3 + 6\psi^2 + 48\right) / 24$$

$$\alpha_{03} = -\left(15\psi^2 - 4\psi - 8\right) / (\psi + 2) \qquad \alpha_{13} = -\left(6\psi^2 + 2\psi - 8\right) / (\psi + 2) \qquad \alpha_{23} = \left(\psi^4 + 4\psi^3 + 3\psi^2 + 24\right) / 24$$

$$\alpha_{04} = \left(5\psi^2 - 2\psi - 3\right) / (\psi + 3) \qquad \alpha_{14} = \left(2\psi^2 + \psi - 3\right) / (\psi + 3) \qquad \alpha_{24} = -\left(\psi^4 + 3\psi^3 + 2\psi^2\right) / 72$$

Table 3 Scheme $E4_{D2}$: 2^{nd} order cut-cell boundary closures for second derivatives with Dirichlet boundary conditions for 4^{th} order interior scheme. 4^{th} order accuracy overall.

$$\alpha_{00} = \left(20\psi^3 + 180\psi^2 + 2050\psi + 450\right) / \left(\psi^5 + 15\psi^4 + 85\psi^3 + 225\psi^2 + 274\psi + 120\right)$$

$$\alpha_{01} = -(77\psi) / 6$$

$$\alpha_{02} = -\left(2\psi^3 - 364\psi^2 + 71\psi + 77\right) / (6\psi + 6)$$

$$\alpha_{03} = \left(4\psi^3 - 346\psi^2 + 118\psi + 107\right) / (3\psi + 6)$$

$$\alpha_{04} = -\left(6\psi^3 - 331\psi^2 + 147\psi + 117\right) / (3\psi + 9)$$

$$\alpha_{05} = \left(8\psi^3 - 319\psi^2 + 164\psi + 122\right) / (6\psi + 24)$$

$$\alpha_{06} = -\left(2\psi^3 - 62\psi^2 + 35\psi + 25\right) / (6\psi + 30)$$

$$\alpha_{10} = 150 / \left(\psi^4 + 12\psi^3 + 49\psi^2 + 78\psi + 40\right)$$

$$\alpha_{11} = -(5\psi) / 4$$

$$\alpha_{12} = \left(75\psi^2 + 71\psi - 154\right) / (12\psi + 12)$$

$$\alpha_{13} = -\left(75\psi^2 + 118\psi - 214\right) / (6\psi + 12)$$

$$\alpha_{14} = (25\psi - 26) / 2$$

$$\alpha_{15} = -\left(75\psi^2 + 164\psi - 244\right) / (12\psi + 48)$$

$$\alpha_{16} = \left(15\psi^2 + 35\psi - 50\right) / (12\psi + 60)$$

$$\alpha_{20} = -\psi / 12$$

$$\alpha_{21} = \left(\psi^6 + 15\psi^5 + 85\psi^4 + 225\psi^3 + 274\psi^2 + 120\psi + 1200\right) / 1440$$

$$\alpha_{22} = -\left(\psi^6 + 14\psi^5 + 71\psi^4 + 154\psi^3 + 120\psi^2 + 360\right) / 288$$

$$\alpha_{23} = \left(\psi^6 + 13\psi^5 + 59\psi^4 + 107\psi^3 + 60\psi^2 - 48\right) / 144$$

$$\alpha_{24} = -\left(\psi^6 + 12\psi^5 + 49\psi^4 + 78\psi^3 + 40\psi^2 - 168\right) / 144$$

$$\alpha_{25} = \left(\psi^6 + 11\psi^5 + 41\psi^4 + 61\psi^3 + 30\psi^2 - 144\right) / 288$$

$$\alpha_{26} = -\left(\psi^6 + 10\psi^5 + 35\psi^4 + 50\psi^3 + 24\psi^2 - 120\right) / 1440$$

$$\alpha_{30} = \psi / 90$$

$$\alpha_{31} = -\left(\psi^6 + 15\psi^5 + 85\psi^4 + 225\psi^3 + 274\psi^2 + 120\psi + 900\right) / 10800$$

$$\alpha_{32} = \left(\psi^6 + 14\psi^5 + 71\psi^4 + 154\psi^3 + 120\psi^2 + 2880\right) / 2160$$

$$\alpha_{33} = -\left(\psi^6 + 13\psi^5 + 59\psi^4 + 107\psi^3 + 60\psi^2 + 2700\right) / 1080$$

$$\alpha_{34} = \left(\psi^6 + 12\psi^5 + 49\psi^4 + 78\psi^3 + 40\psi^2 + 1440\right) / 1080$$

$$\alpha_{35} = -\left(\psi^6 + 11\psi^5 + 41\psi^4 + 61\psi^3 + 30\psi^2 + 180\right) / 2160$$

$$\alpha_{36} = \left(\psi^6 + 10\psi^5 + 35\psi^4 + 50\psi^3 + 24\psi^2\right) / 10800$$

Table 4 Scheme $E6_{D2}$: 4^{th} order cut-cell boundary closures for second derivatives with Dirichlet boundary conditions for 6^{th} order interior scheme. 6^{th} order accuracy overall.

$$\alpha_{00} = \left(42\psi^5 + 840\psi^4 + 6440\psi^3 + 23520\psi^2 + 153006\psi + 26264\right) / \left(\psi^7 + 28\psi^6 + 322\psi^5 + 1960\psi^4 + 6769\psi^3 + 13132\psi^2 + 13068\psi + 5040\right)$$

$$\alpha_{01} = -(223\psi)/10$$

$$\alpha_{02} = -\left(6\psi^5 + 135\psi^4 + 1180\psi^3 - 51201\psi^2 + 10208\psi + 8028\right)/(360\psi + 360)$$

$$\alpha_{03} = \left(3\psi^5 + 65\psi^4 + 540\psi^3 - 11919\psi^2 + 3929\psi + 2637\right)/(30\psi + 60)$$

$$\alpha_{04} = -\left(6\psi^5 + 125\psi^4 + 988\psi^3 - 15075\psi^2 + 6224\psi + 3796\right)/(24\psi + 72)$$

$$\alpha_{05} = \left(6\psi^5 + 120\psi^4 + 904\psi^3 - 10881\psi^2 + 5090\psi + 2952\right)/(18\psi + 72)$$

$$\alpha_{06} = -\left(30\psi^5 + 575\psi^4 + 4140\psi^3 - 42321\psi^2 + 21440\psi + 12060\right)/(120\psi + 600)$$

$$\alpha_{07} = \left(3\psi^5 + 55\psi^4 + 380\psi^3 - 3453\psi^2 + 1849\psi + 1019\right)/(30\psi + 180)$$

$$\alpha_{08} = -\left(6\psi^5 + 105\psi^4 + 700\psi^3 - 5823\psi^2 + 3248\psi + 1764\right)/(360\psi + 2520)$$

$$\alpha_{10} = (1960\psi + 26264)/\left(\psi^7 + 28\psi^6 + 322\psi^5 + 1960\psi^4 + 6769\psi^3 + 13132\psi^2 + 13068\psi + 5040\right)$$

$$\alpha_{11} = -(7\psi)/18$$

$$\alpha_{12} = \left(245\psi^2 + 1276\psi - 2007\right)/(90\psi + 90)$$

$$\alpha_{13} = -\left(490\psi^2 + 3929\psi - 5274\right)/(60\psi + 120)$$

$$\alpha_{14} = \left(245\psi^2 + 2334\psi - 2847\right)/(18\psi + 54)$$

$$\alpha_{15} = -\left(245\psi^2 + 2545\psi - 2952\right)/(18\psi + 72)$$

$$\alpha_{16} = \left(49\psi^2 + 536\psi - 603\right)/(6\psi + 30)$$

$$\alpha_{17} = -\left(490\psi^2 + 5547\psi - 6114\right)/(180\psi + 1080)$$

$$\alpha_{18} = \left(35\psi^2 + 406\psi - 441\right)/(90\psi + 630)$$

$$\alpha_{20} = -(11\psi)/180$$

$$\alpha_{21} = \left(11\psi^8 + 308\psi^7 + 3542\psi^6 + 21560\psi^5 + 74459\psi^4 + 144452\psi^3 + 143748\psi^2 + 55440\psi + 635040\right)/907200$$

$$\alpha_{22} = -\left(11\psi^8 + 297\psi^7 + 3245\psi^6 + 18315\psi^5 + 56144\psi^4 + 88308\psi^3 + 55440\psi^2 + 50400\right)/129600$$

$$\alpha_{23} = \left(11\psi^8 + 286\psi^7 + 2970\psi^6 + 15620\psi^5 + 43219\psi^4 + 58014\psi^3 + 27720\psi^2 - 116640\right)/43200$$

$$\alpha_{24} = -\left(11\psi^8 + 275\psi^7 + 2717\psi^6 + 13409\psi^5 + 34232\psi^4 + 41756\psi^3 + 18480\psi^2 - 123120\right)/25920$$

$$\alpha_{25} = \left(11\psi^8 + 264\psi^7 + 2486\psi^6 + 11616\psi^5 + 27995\psi^4 + 32472\psi^3 + 13860\psi^2 - 96480\right)/25920$$

$$\alpha_{26} = -\left(11\psi^8 + 253\psi^7 + 2277\psi^6 + 10175\psi^5 + 23584\psi^4 + 26532\psi^3 + 11088\psi^2 - 77760\right)/43200$$

$$\alpha_{27} = \left(11\psi^8 + 242\psi^7 + 2090\psi^6 + 9020\psi^5 + 20339\psi^4 + 22418\psi^3 + 9240\psi^2 - 64800\right)/129600$$

$$\alpha_{28} = -\left(11\psi^8 + 231\psi^7 + 1925\psi^6 + 8085\psi^5 + 17864\psi^4 + 19404\psi^3 + 7920\psi^2 - 55440\right)/907200$$

$$\alpha_{30} = \psi/90$$

$$\alpha_{31} = -\left(\psi^8 + 28\psi^7 + 322\psi^6 + 1960\psi^5 + 6769\psi^4 + 13132\psi^3 + 13068\psi^2 + 5040\psi + 27720\right)/453600$$

$$\alpha_{32} = \left(\psi^8 + 27\psi^7 + 295\psi^6 + 1665\psi^5 + 5104\psi^4 + 8028\psi^3 + 5040\psi^2 + 77040\right)/64800$$

$$\alpha_{33} = -\left(\psi^8 + 26\psi^7 + 270\psi^6 + 1420\psi^5 + 3929\psi^4 + 5274\psi^3 + 2520\psi^2 + 45360\right)/21600$$

$$\alpha_{34} = \left(\psi^8 + 25\psi^7 + 247\psi^6 + 1219\psi^5 + 3112\psi^4 + 3796\psi^3 + 1680\psi^2 + 9360\right)/12960$$

$$\alpha_{35} = -\left(\psi^8 + 24\psi^7 + 226\psi^6 + 1056\psi^5 + 2545\psi^4 + 2952\psi^3 + 1260\psi^2 - 6120\right)/12960$$

$$\alpha_{36} = \left(\psi^8 + 23\psi^7 + 207\psi^6 + 925\psi^5 + 2144\psi^4 + 2412\psi^3 + 1008\psi^2 - 6480\right)/21600$$

$$\alpha_{37} = -\left(\psi^8 + 22\psi^7 + 190\psi^6 + 820\psi^5 + 1849\psi^4 + 2038\psi^3 + 840\psi^2 - 5760\right)/64800$$

$$\alpha_{38} = \left(\psi^8 + 21\psi^7 + 175\psi^6 + 735\psi^5 + 1624\psi^4 + 1764\psi^3 + 720\psi^2 - 5040\right)/453600$$

Table 5 Scheme $E8_{D2}$: 6^{th} order cut-cell closures for second derivatives with Dirichlet boundary conditions for 8^{th} order interior scheme. 8^{th} order accuracy overall.

$$\alpha_{40} = -\psi/560$$
$$\alpha_{41} = \left(\psi^8 + 28\psi^7 + 322\psi^6 + 1960\psi^5 + 6769\psi^4 + 13132\psi^3 + 13068\psi^2 + 5040\psi + 31360\right)/2822400$$
$$\alpha_{42} = -\left(\psi^8 + 27\psi^7 + 295\psi^6 + 1665\psi^5 + 5104\psi^4 + 8028\psi^3 + 5040\psi^2 + 60480\right)/403200$$
$$\alpha_{43} = \left(\psi^8 + 26\psi^7 + 270\psi^6 + 1420\psi^5 + 3929\psi^4 + 5274\psi^3 + 2520\psi^2 + 201600\right)/134400$$
$$\alpha_{44} = -\left(\psi^8 + 25\psi^7 + 247\psi^6 + 1219\psi^5 + 3112\psi^4 + 3796\psi^3 + 1680\psi^2 + 219520\right)/80640$$
$$\alpha_{45} = \left(\psi^8 + 24\psi^7 + 226\psi^6 + 1056\psi^5 + 2545\psi^4 + 2952\psi^3 + 1260\psi^2 + 120960\right)/80640$$
$$\alpha_{46} = -\left(\psi^8 + 23\psi^7 + 207\psi^6 + 925\psi^5 + 2144\psi^4 + 2412\psi^3 + 1008\psi^2 + 20160\right)/134400$$
$$\alpha_{47} = \left(\psi^8 + 22\psi^7 + 190\psi^6 + 820\psi^5 + 1849\psi^4 + 2038\psi^3 + 840\psi^2 + 4480\right)/403200$$
$$\alpha_{48} = -\left(\psi^8 + 21\psi^7 + 175\psi^6 + 735\psi^5 + 1624\psi^4 + 1764\psi^3 + 720\psi^2\right)/2822400$$

Table 5 (Continued) Scheme $E8_{D2}$: 6^{th} order cut-cell boundary closures for second derivatives with Dirichlet boundary conditions for 8^{th} order interior scheme. 8^{th} order accuracy overall.

$$\alpha_0' = -3 \qquad \alpha_1' = -3(1-\psi)$$
$$\alpha_{00} = -\frac{9\psi^2 + 54\psi + 21}{\psi^3 + 6\psi^2 + 11\psi + 6} \qquad \alpha_{10} = \frac{9\psi^3 + 27\psi^2 + 9\psi - 21}{\psi^3 + 6\psi^2 + 11\psi + 6} \qquad \alpha_{20} = -\psi/12$$
$$\alpha_{01} = 4\psi \qquad \alpha_{11} = -2\psi \qquad \alpha_{21} = \left(\psi^4 + 6\psi^3 + 11\psi^2 + 6\psi + 72\right)/72$$
$$\alpha_{02} = -\left(21\psi^2 - 11\psi - 8\right)/(2\psi + 2) \qquad \alpha_{12} = -\left(3\psi^3 + \psi - 8\right)/(2\psi + 2) \qquad \alpha_{22} = -\left(\psi^4 + 5\psi^3 + 6\psi^2 + 48\right)/24$$
$$\alpha_{03} = \left(9\psi^2 - 8\psi - 1\right)/(\psi + 2) \qquad \alpha_{13} = \left(3\psi^3 + 3\psi^2 - 5\psi - 1\right)/(\psi + 2) \qquad \alpha_{23} = \left(\psi^4 + 4\psi^3 + 3\psi^2 + 24\right)/24$$
$$\alpha_{04} = -\left(5\psi^2 - 5\psi\right)/(2\psi + 6) \qquad \alpha_{14} = -\left(3\psi^3 + 2\psi^2 - 5\psi\right)/(2\psi + 6) \qquad \alpha_{24} = -\left(\psi^4 + 3\psi^3 + 2\psi^2\right)/72$$

Table 6 Scheme $E4_{N2}$: 2^{nd} order cut-cell boundary closures for second derivatives with Neumann boundary conditions for 4^{th} order interior scheme. 4^{th} order accuracy overall.

$$\alpha'_0 = -25/6$$

$$\alpha_{00} = -\left(125\psi^4 + 1380\psi^3 + 5295\psi^2 + 13950\psi + 4150\right)/\left(6\psi^5 + 90\psi^4 + 510\psi^3 + 1350\psi^2 + 1644\psi + 720\right)$$

$$\alpha_{01} = 8\psi$$

$$\alpha_{02} = \left(25\psi^4 + 302\psi^3 - 4489\psi^2 + 2146\psi + 1152\right)/(144\psi + 144)$$

$$\alpha_{03} = -\left(25\psi^4 + 277\psi^3 - 1873\psi^2 + 1259\psi + 216\right)/(36\psi + 72)$$

$$\alpha_{04} = \left(25\psi^4 + 252\psi^3 - 1127\psi^2 + 774\psi + 64\right)/(24\psi + 72)$$

$$\alpha_{05} = -\left(25\psi^4 + 227\psi^3 - 811\psi^2 + 541\psi + 18\right)/(36\psi + 144)$$

$$\alpha_{06} = \left(25\psi^4 + 202\psi^3 - 637\psi^2 + 410\psi\right)/(144\psi + 720)$$

$$\alpha'_1 = (5\psi)/12 - (25(1-\psi))/6$$

$$\alpha_{10} = \left(275\psi^5 + 3050\psi^4 + 11025\psi^3 + 12000\psi^2 - 2630\psi - 8300\right)/\left(12\psi^5 + 180\psi^4 + 1020\psi^3 + 2700\psi^2 + 3288\psi + 1440\right)$$

$$\alpha_{11} = -(10\psi)/3$$

$$\alpha_{12} = -\left(55\psi^5 + 720\psi^4 + 3205\psi^3 + 120\psi^2 - 2804\psi - 2304\right)/(288\psi + 288)$$

$$\alpha_{13} = \left(55\psi^5 + 665\psi^4 + 2595\psi^3 + 535\psi^2 - 3466\psi - 432\right)/(72\psi + 144)$$

$$\alpha_{14} = -\left(55\psi^5 + 610\psi^4 + 2095\psi^3 + 240\psi^2 - 2876\psi - 128\right)/(48\psi + 144)$$

$$\alpha_{15} = \left(55\psi^5 + 555\psi^4 + 1705\psi^3 + 105\psi^2 - 2384\psi - 36\right)/(72\psi + 288)$$

$$\alpha_{16} = -\left(55\psi^5 + 500\psi^4 + 1425\psi^3 + 40\psi^2 - 2020\psi\right)/(288\psi + 1440)$$

$$\alpha'_2 = (5(1-\psi))/12$$

$$\alpha_{20} = -\psi/12$$

$$\alpha_{21} = \left(\psi^6 - 10\psi^5 - 190\psi^4 - 750\psi^3 - 701\psi^2 + 1000\psi + 2570\right)/1440$$

$$\alpha_{22} = -\left(\psi^6 - 11\psi^5 - 184\psi^4 - 631\psi^3 - 355\psi^2 + 940\psi + 960\right)/288$$

$$\alpha_{23} = \left(\psi^6 - 12\psi^5 - 176\psi^4 - 518\psi^3 - 125\psi^2 + 770\psi + 252\right)/144$$

$$\alpha_{24} = -\left(\psi^6 - 13\psi^5 - 166\psi^4 - 417\psi^3 - 5\psi^2 + 580\psi + 32\right)/144$$

$$\alpha_{25} = \left(\psi^6 - 14\psi^5 - 154\psi^4 - 334\psi^3 + 35\psi^2 + 460\psi + 6\right)/288$$

$$\alpha_{26} = -\left(\psi^6 - 15\psi^5 - 140\psi^4 - 275\psi^3 + 49\psi^2 + 380\psi\right)/1440$$

$$\alpha_{30} = \psi/90$$

$$\alpha_{31} = -\left(\psi^6 + 15\psi^5 + 85\psi^4 + 225\psi^3 + 274\psi^2 + 120\psi + 900\right)/10800$$

$$\alpha_{32} = \left(\psi^6 + 14\psi^5 + 71\psi^4 + 154\psi^3 + 120\psi^2 + 2880\right)/2160$$

$$\alpha_{33} = -\left(\psi^6 + 13\psi^5 + 59\psi^4 + 107\psi^3 + 60\psi^2 + 2700\right)/1080$$

$$\alpha_{34} = \left(\psi^6 + 12\psi^5 + 49\psi^4 + 78\psi^3 + 40\psi^2 + 1440\right)/1080$$

$$\alpha_{35} = -\left(\psi^6 + 11\psi^5 + 41\psi^4 + 61\psi^3 + 30\psi^2 + 180\right)/2160$$

$$\alpha_{36} = \left(\psi^6 + 10\psi^5 + 35\psi^4 + 50\psi^3 + 24\psi^2\right)/10800$$

Table 7 Scheme $E6_{N2}$: 4^{th} order cut-cell boundary closures for second derivatives with Neumann boundary conditions for 6^{th} order interior scheme. 6^{th} order accuracy overall.

$$\alpha'_0 = -49/10$$

$$\alpha_{00} = -\left(343\psi^6 + 7812\psi^5 + 70490\psi^4 + 319760\psi^3 + 759843\psi^2 + 1485596\psi + 377692\right) / \left(10\psi^7 + 280\psi^6 + 3220\psi^5 + 19600\psi^4 + 67690\psi^3 + 131320\psi^2 + 130680\psi + 50400\right)$$

$$\alpha_{01} = 12\psi$$

$$\alpha_{02} = \left(49\psi^6 + 1203\psi^5 + 11755\psi^4 + 57985\psi^3 - 454604\psi^2 + 189212\psi + 86400\right) / (7200\psi + 7200)$$

$$\alpha_{03} = -\left(49\psi^6 + 1154\psi^5 + 10630\psi^4 + 47980\psi^3 - 195079\psi^2 + 101266\psi + 18000\right) / (1200\psi + 2400)$$

$$\alpha_{04} = \left(49\psi^6 + 1105\psi^5 + 9603\psi^4 + 39971\psi^3 - 122252\psi^2 + 61524\psi + 6400\right) / (480\psi + 1440)$$

$$\alpha_{05} = -\left(49\psi^6 + 1056\psi^5 + 8674\psi^4 + 33664\psi^3 - 89855\psi^2 + 42848\psi + 2700\right) / (360\psi + 1440)$$

$$\alpha_{06} = \left(49\psi^6 + 1007\psi^5 + 7843\psi^4 + 28765\psi^3 - 71404\psi^2 + 32428\psi + 1152\right) / (480\psi + 2400)$$

$$\alpha_{07} = -\left(49\psi^6 + 958\psi^5 + 7110\psi^4 + 24980\psi^3 - 59399\psi^2 + 25902\psi + 400\right) / (1200\psi + 7200)$$

$$\alpha_{08} = \left(49\psi^6 + 909\psi^5 + 6475\psi^4 + 22015\psi^3 - 50924\psi^2 + 21476\psi\right) / (7200\psi + 50400)$$

$$\alpha'_1 = (77\psi)/180 - (49(1-\psi))/10$$

$$\alpha_{10} = \left(6713\psi^7 + 154938\psi^6 + 1395814\psi^5 + 6098540\psi^4 + 12559533\psi^3 + 7276402\psi^2 - 7563276\psi - 6798456\right) / \left(180\psi^7 + 5040\psi^6 + 57960\psi^5 + 352800\psi^4 + 1218420\psi^3 + 2363760\psi^2 + 2352240\psi + 907200\right)$$

$$\alpha_{11} = -(203\psi)/60$$

$$\alpha_{12} = -\left(959\psi^7 + 25011\psi^6 + 259091\psi^5 + 1336545\psi^4 + 3426206\psi^3 + 127764\psi^2 - 4084776\psi - 1555200\right) / (129600\psi + 129600)$$

$$\alpha_{13} = \left(959\psi^7 + 24052\psi^6 + 235998\psi^5 + 1123640\psi^4 + 2515471\psi^3 + 57708\psi^2 - 3649428\psi - 324000\right) / (21600\psi + 43200)$$

$$\alpha_{14} = -\left(959\psi^7 + 23093\psi^6 + 214823\psi^5 + 951167\psi^4 + 1909250\psi^3 - 127540\psi^2 - 2857272\psi - 115200\right) / (8640\psi + 25920)$$

$$\alpha_{15} = \left(959\psi^7 + 22134\psi^6 + 195566\psi^5 + 813372\psi^4 + 1509263\psi^3 - 181062\psi^2 - 2311524\psi - 48600\right) / (6480\psi + 25920)$$

$$\alpha_{16} = -\left(959\psi^7 + 21175\psi^6 + 178227\psi^5 + 704501\psi^4 + 1240246\psi^3 - 191772\psi^2 - 1932552\psi - 20736\right) / (8640\psi + 43200)$$

$$\alpha_{17} = \left(959\psi^7 + 20216\psi^6 + 162806\psi^5 + 618800\psi^4 + 1049951\psi^3 - 187936\psi^2 - 1657596\psi - 7200\right) / (21600\psi + 129600)$$

$$\alpha_{18} = -\left(959\psi^7 + 19257\psi^6 + 149303\psi^5 + 550515\psi^4 + 909146\psi^3 - 179172\psi^2 - 1450008\psi\right) / (129600\psi + 907200)$$

$$\alpha'_2 = (77(1-\psi))/180 - (7\psi)/90$$

$$\alpha_{20} = -(473\psi)/1800$$

$$\alpha_{21} = \left(473\psi^8 + 6874\psi^7 + 4816\psi^6 - 408660\psi^5 - 2692963\psi^4 - 6231134\psi^3 - 2082686\psi^2 + 10715320\psi + 16412760\right) / 9072000$$

$$\alpha_{22} = -\left(473\psi^8 + 6401\psi^7 - 2495\psi^6 - 429965\psi^5 - 2510658\psi^4 - 5008476\psi^3 - 436800\psi^2 + 7776720\psi + 4384800\right) / 1296000$$

$$\alpha_{23} = \left(473\psi^8 + 5928\psi^7 - 8860\psi^6 - 436720\psi^5 - 2270883\psi^4 - 3857968\psi^3 + 669270\psi^2 + 5828760\psi + 774000\right) / 432000$$

$$\alpha_{24} = -\left(473\psi^8 + 5455\psi^7 - 14279\psi^6 - 431763\psi^5 - 2014234\psi^4 - 2945732\psi^3 + 1074640\psi^2 + 4317040\psi + 62400\right) / 259200$$

$$\alpha_{25} = \left(473\psi^8 + 4982\psi^7 - 18752\psi^6 - 417932\psi^5 - 1769955\psi^4 - 2299074\psi^3 + 1102290\psi^2 + 3399480\psi + 5400\right) / 259200$$

$$\alpha_{26} = -\left(473\psi^8 + 4509\psi^7 - 22279\psi^6 - 398065\psi^5 - 1555938\psi^4 - 1863244\psi^3 + 1039584\psi^2 + 2797200\psi - 1440\right) / 432000$$

$$\alpha_{27} = \left(473\psi^8 + 4036\psi^7 - 24860\psi^6 - 375000\psi^5 - 1378723\psi^4 - 1558196\psi^3 + 959350\psi^2 + 2374120\psi - 1200\right) / 1296000$$

$$\alpha_{28} = -\left(473\psi^8 + 3563\psi^7 - 26495\psi^6 - 351575\psi^5 - 1233498\psi^4 - 1335348\psi^3 + 881520\psi^2 + 2061360\psi\right) / 9072000$$

Table 8 Scheme $E8_{N2}$: 6^{th} order cut-cell boundary closures for second derivatives with Neumann boundary conditions for 8^{th} order interior scheme. 8^{th} order accuracy overall.

$$\alpha_3' = -(7(1-\psi))/90$$

$$\alpha_{30} = \psi/90$$

$$\alpha_{31} = -\left(\psi^8 - 21\psi^7 - 805\psi^6 - 8134\psi^5 - 36841\psi^4 - 74137\psi^3 - 28631\psi^2 + 97412\psi + 119196\right)/453600$$

$$\alpha_{32} = \left(\psi^8 - 22\psi^7 - 790\psi^6 - 7526\psi^5 - 31191\psi^4 - 52536\psi^3 - 168\psi^2 + 77112\psi + 112320\right)/64800$$

$$\alpha_{33} = -\left(\psi^8 - 23\psi^7 - 773\psi^6 - 6938\psi^5 - 26381\psi^4 - 37475\psi^3 + 11193\psi^2 + 56196\psi + 63000\right)/21600$$

$$\alpha_{34} = \left(\psi^8 - 24\psi^7 - 754\psi^6 - 6376\psi^5 - 22375\psi^4 - 27424\psi^3 + 13888\psi^2 + 41384\psi + 21120\right)/12960$$

$$\alpha_{35} = -\left(\psi^8 - 25\psi^7 - 733\psi^6 - 5846\psi^5 - 19113\psi^4 - 20925\psi^3 + 13377\psi^2 + 32508\psi + 2700\right)/12960$$

$$\alpha_{36} = \left(\psi^8 - 26\psi^7 - 710\psi^6 - 5354\psi^5 - 16511\psi^4 - 16712\psi^3 + 12264\psi^2 + 26712\psi + 576\right)/21600$$

$$\alpha_{37} = -\left(\psi^8 - 27\psi^7 - 685\psi^6 - 4906\psi^5 - 14461\psi^4 - 13831\psi^3 + 11137\psi^2 + 22652\psi + 120\right)/64800$$

$$\alpha_{38} = \left(\psi^8 - 28\psi^7 - 658\psi^6 - 4508\psi^5 - 12831\psi^4 - 11760\psi^3 + 10128\psi^2 + 19656\psi\right)/453600$$

$$\alpha_{40} = -\psi/560$$

$$\alpha_{41} = \left(\psi^8 + 28\psi^7 + 322\psi^6 + 1960\psi^5 + 6769\psi^4 + 13132\psi^3 + 13068\psi^2 + 5040\psi + 31360\right)/2822400$$

$$\alpha_{42} = -\left(\psi^8 + 27\psi^7 + 295\psi^6 + 1665\psi^5 + 5104\psi^4 + 8028\psi^3 + 5040\psi^2 + 60480\right)/403200$$

$$\alpha_{43} = \left(\psi^8 + 26\psi^7 + 270\psi^6 + 1420\psi^5 + 3929\psi^4 + 5274\psi^3 + 2520\psi^2 + 201600\right)/134400$$

$$\alpha_{44} = -\left(\psi^8 + 25\psi^7 + 247\psi^6 + 1219\psi^5 + 3112\psi^4 + 3796\psi^3 + 1680\psi^2 + 219520\right)/80640$$

$$\alpha_{45} = \left(\psi^8 + 24\psi^7 + 226\psi^6 + 1056\psi^5 + 2545\psi^4 + 2952\psi^3 + 1260\psi^2 + 120960\right)/80640$$

$$\alpha_{46} = -\left(\psi^8 + 23\psi^7 + 207\psi^6 + 925\psi^5 + 2144\psi^4 + 2412\psi^3 + 1008\psi^2 + 20160\right)/134400$$

$$\alpha_{47} = \left(\psi^8 + 22\psi^7 + 190\psi^6 + 820\psi^5 + 1849\psi^4 + 2038\psi^3 + 840\psi^2 + 4480\right)/403200$$

$$\alpha_{48} = -\left(\psi^8 + 21\psi^7 + 175\psi^6 + 735\psi^5 + 1624\psi^4 + 1764\psi^3 + 720\psi^2\right)/2822400$$

Table 8 (Continued) Scheme $E8_{N2}$: 6^{th} order cut-cell boundary closures for second derivatives with Neumann boundary conditions for 8^{th} order interior scheme. 8^{th} order accuracy overall.

Acknowledgments

This work was supported by the US Department of Energy through the Los Alamos National Laboratory. Los Alamos National Laboratory is operated by Triad National Security, LLC, for the National Nuclear Security Administration of U.S. Department of Energy (Contract No. 89233218CNA000001). Computational resources were provided by the LANL Institutional Computing (IC) Program.

References

[1] Clarke, D., Hassan, H., and Salas, M., "Euler calculations for multielement airfoils using Cartesian grids," *AIAA Journal*, Vol. 24, No. 3, 1986, pp. 353–358.

[2] Mittal, R., and Iaccarino, G., "Immersed boundary methods," *Annual Review of Fluid Mechanics*, Vol. 37, No. 1, 2005, pp. 239–261. doi:10.1146/annurev.fluid.37.061903.175743.

[3] Quirk, J., "An alternative to unstructured grids for computing gas dynamic flows around arbitrarily complex two-dimensional bodies," *Computers & Fluids*, Vol. 23, No. I, 1994, pp. 125–142.

[4] Berger, M., and R, L., "An Adaptive Cartesian Mesh Algorithm for the Euler Equations in Arbitrary Geometries," *AIAA Paper 89-1930*, 1989.

[5] Chiang, B., Y-L; van Leer, and Powell, K., "Simulation of Unsteady Inviscid Flow on an Adaptively Refined Cartesian Grid," *AIAA Paper 92-0443*, 1992.

[6] Pember, R., and Bell, J., "An adaptive Cartesian grid method for unsteady compressible flow in irregular regions," *Journal of Computational Physics*, Vol. 120, 1995, pp. 278–304.

[7] Udaykumar, H., Shyy, W., and Rao, M., "ELAFINT: a mixed Eulerian?Lagrangian method for fluid flows with complex and moving boundaries," *International Journal for Numerical Methods in Fluids*, Vol. 22, 1996, pp. 691–712.

[8] Udaykumar, H., Kan, H.-C., Shyy, W., and Tran-Son-Tay, R., "Multiphase dynamics in arbitrary geometries on fixed Cartesian grids," *Journal of Computational Physics*, Vol. 137, No. 2, 1997, pp. 366–405. doi:10.1006/jcph.1997.5805.

[9] Udaykumar, H. S., Mittal, R., and Rampunggoon, P., "Interface tracking finite volume method for complex solid-fluid interactions on fixed meshes," *Communications in Numerical Methods in Engineering*, Vol. 18, No. 2, 2001, pp. 89–97. doi:10.1002/cnm.468.

[10] Udaykumar, H., Mittal, R., Rampunggoon, P., and Khanna, A., "A sharp interface Cartesian grid method for simulating flows with complex moving boundaries," *Journal of Computational Physics*, Vol. 174, No. 1, 2001, pp. 345–380. doi: 10.1006/jcph.2001.6916.

[11] Yang, G., Causon, D., Ingram, D., Saunders, R., and Batten, P., "A Cartesian cut cell method for compressible flows. A. Static body problems," *Aerospace Engineering & Technology*, Vol. 101, No. 1002, 1997, pp. 47–56.

[12] Yang, G., Causon, D., and Ingram, D., "Calculation of compressible flows about complex moving geometries using a three-dimensional Cartesian cut cell method," *International Journal for Numerical Methods in Fluids*, Vol. 33, 2000, pp. 1121–1151.

[13] Almgren, A., Bell, J., Colella, P., and Marthaler, T., "A Cartesian grid projection method for the incompressible Euler equations in complex geometries," *SIAM Journal on Scientific Computing*, Vol. 18, No. 5, 1997, pp. 1289–1309.

[14] Ye, T., Mittal, R., Udaykumar, H., and Shyy, W., "An accurate Cartesian grid method for viscous incompressible flows with complex immersed boundaries," *Journal of Computational Physics*, Vol. 156, No. 2, 1999, pp. 209–240. doi:10.1006/jcph. 1999.6356.

[15] Chung, M.-H., "A level set approach for computing solutions to inviscid compressible flow with moving solid boundary using fixed Cartesian grids," *International Journal for Numerical Methods in Fluids*, Vol. 36, No. 4, 2001, pp. 373–389. doi:10.1002/fld.32.

[16] McCorquodale, P., Colella, P., and Johansen, H., "A Cartesian grid embedded boundary method for the heat equation on irregular domains," *Journal of Computational Physics*, Vol. 173, No. 2, 2001, pp. 620–635. doi:10.1006/jcph.2001.6900.

[17] Schwartz, P., Barad, M., Colella, P., and Ligocki, T., "A Cartesian grid embedded boundary method for the heat equation and Poisson's equation in three dimensions," *Journal of Computational Physics*, Vol. 211, No. 2, 2006, pp. 531–550. doi:10.1016/j.jcp.2005.06.010.

[18] Kirkpatrick, M. P., Armfield, S. W., and Kent, J. H., "A representation of curved boundaries for the solution of the Navier-Stokes equations on a staggered three-dimensional Cartesian grid," *Journal of Computational Physics*, Vol. 184, 2003, pp. 1–36.

[19] Chung, M.-H., "Cartesian cut cell approach for simulating incompressible flows with rigid bodies of arbitrary shape," *Computers & Fluids*, Vol. 35, No. 6, 2006, pp. 607–623. doi:10.1016/j.compfluid.2005.04.005.

[20] Hartmann, D., Meinke, M., and Schröder, W., "A strictly conservative Cartesian cut-cell method for compressible viscous flows on adaptive grids," *Computer Methods in Applied Mechanics and Engineering*, Vol. 200, No. 9-12, 2011, pp. 1038–1052. doi:10.1016/j.cma.2010.05.015.

[21] Meyer, M., Devesa, A., Hickel, S., Hu, X., and Adams, N., "A conservative immersed interface method for Large-Eddy Simulation of incompressible flows," *Journal of Computational Physics*, Vol. 229, No. 18, 2010, pp. 6300–6317. doi: 10.1016/j.jcp.2010.04.040.

[22] Seo, J. H., and Mittal, R., "A sharp-interface immersed boundary method with improved mass conservation and reduced spurious pressure oscillations." *Journal of Computational Physics*, Vol. 230, No. 19, 2011, pp. 7347–7363. doi:10.1016/j.jcp.2011.06.003.

[23] Crockett, R., Colella, P., and Graves, D., "A Cartesian grid embedded boundary method for solving the Poisson and heat equations with discontinuous coefficients in three dimensions," *Journal of Computational Physics*, Vol. 230, No. 7, 2011, pp. 2451–2469. doi:10.1016/j.jcp.2010.12.017.

[24] Barton, P., Obadia, B., and Drikakis, D., "A conservative level-set based method for compressible solid/fluid problems on fixed grids," *Journal of Computational Physics*, Vol. 230, No. 21, 2011, pp. 7867–7890. doi:10.1016/j.jcp.2011.07.008.

[25] Monasse, L., Daru, V., Mariotti, C., Piperno, S., and Tenaud, C., "A conservative coupling algorithm between a compressible flow and a rigid body using an embedded boundary method," *Journal of Computational Physics*, Vol. 231, No. 7, 2012, pp. 2977–2994. doi:10.1016/j.jcp.2012.01.002.

[26] Cecere, D., and Giacomazzi, E., "ScienceDirect An immersed volume method for Large Eddy Simulation of compressible flows using a staggered-grid approach," *Comput. Methods Appl. Mech. Engrg.*, Vol. 280, 2014, pp. 1–27. doi:10.1016/j.cma.2014.07.018.

[27] Schneiders, L., Hartmann, D., Meinke, M., and Schröder, W., "An accurate moving boundary formulation in cut-cell methods," *Journal of Computational Physics*, Vol. 235, 2013, pp. 786–809. doi:10.1016/j.jcp.2012.09.038.

[28] Brehm, C., and Fasel, H., "A novel concept for the design of immersed interface methods," *Journal of Computational Physics*, Vol. 242, 2013, pp. 234–267. doi:10.1016/j.jcp.2013.01.027.

[29] Schneiders, L., Günther, C., Meinke, M., and Schröder, W., "An efficient conservative cut-cell method for rigid bodies interacting with viscous compressible flows," *Journal of Computational Physics*, Vol. 311, 2016, pp. 62–86. doi:10.1016/j.jcp.2016.01.026.

[30] Brehm, C., Hader, C., and Fasel, H., "A locally stabilized immersed boundary method for the compressible Navier?Stokes equations," *Journal of Computational Physics*, Vol. 295, 2015, pp. 475–504. doi:10.1016/j.jcp.2015.04.023.

[31] Muralidharan, B., and Menon, S., "A high-order adaptive Cartesian cut-cell method for simulation of compressible viscous flow over immersed bodies," *Journal of Computational Physics*, Vol. 321, 2016, pp. 342–368. doi:10.1016/j.jcp.2016.05.050.

[32] Brady, P., and Livescu, D., "Foundations for High-Order, Conservative Cut-Cell Methods: Stable Derivatives on Degenerate Meshes," *J. Comput. Phys.*, Vol. Submitted, 2018.

[33] Brady, P., and Livescu, D., "High-Order, Stable, and Conservative Boundary Schemes for Central and Compact Finite Differences," *Computers & Fluids*, Vol. Submitted, 2018.

[34] Carpenter, M. H., Gottlieb, D., and Abarbanel, S., "The Stability of Numerical Boundary Treatments for Compact High-Order Finite-Difference Schemes," *J. Comput. Phys.*, Vol. 108, No. 2, 1993, pp. 272–295. doi:10.1006/jcph.1993.1182.

[35] Strang, G., *Linear Algebra and its Applications*, Thomson Brooks/Cole, 2006.

[36] Yee, H. C., Sandham, N. D., and Djomehri, M. J., "Low-dissipative high-order shock-capturing methods using characteristic-based filters," *J. Comput. Phys.*, Vol. 150, No. May 1998, 1999, pp. 199–238.

[37] Kim, J. W., "Optimised boundary compact finite difference schemes for computational aeroacoustics," *Journal of Computational Physics*, Vol. 225, No. 1, 2007, pp. 995–1019. doi:10.1016/j.jcp.2007.01.008.

[38] Turner, J. M., Haeri, S., and Kim, J. W., "Improving the boundary efficiency of a compact finite difference scheme through optimising its composite template," *Computers & Fluids*, Vol. 138, 2016, pp. 9–25. doi:10.1016/j.compfluid.2016.08.007.